Fermi National Accelerator Laboratory

CERN-TH.5584/89
FERMILAB-PUB-89/244-T
December 1989

The Decay of the Z Boson into Four Massive Fermions

E. W. N. Glover,

Fermi National Accelerator Laboratory,
P. O. Box 500, Batavia, IL 60510, U.S.A.

R. Kleiss,

TH Division, CERN, CH1211 Geneve 23, Switzerland

and

J. J. van der Bij,

Inst. for Theor. Physics, University of Amsterdam,
Valckenierstr. 65, 1018 XE Amsterdam, The Netherlands.

ABSTRACT

We calculate the partial width for the tree level decay of the Z boson into four massive fermions at $O(\alpha^2)$ and $O(\alpha_s^2)$. Analytic expressions for the helicity amplitudes are presented. We also present 'observable' widths for the case when the fermions are energetic and well separated, and make a comparison between the massive and massless matrix elements in this region. We make a direct comparison between the four fermion decay and the production and decay of the Higgs boson via the Bjorken mechanism, $Z \to H\mu^+\mu^- \to q\bar{q}\mu^+\mu^-$. Provided the detector resolution is good, $\Delta m_{q\bar{q}} \sim$ few GeV, the Higgs signal stands clearly above the four fermion background for all Higgs boson masses considered.

Operated by Universities Research Association Inc. under contract with the United States Department of Energy

1 Introduction

Although the Z boson was first discovered in 1983 [1], it is only recently that its properties have begun to be studied in detail by experiments at LEP and SLC. With only a few thousand events, the four LEP experiments have measured the mass, M_Z and width, Γ_Z with a precision that surpasses that previously achieved. As the number of Z events rapidly increases, new, hitherto unobserved, decay modes will become accessible and may directly or indirectly hint at new physics. Since new physics tends to manifest itself as multi-particle final states consisting of the known leptons and hadrons, it is important to have a good understanding of multi-particle decays within the standard model.

In this paper we will be concerned with the decay of the Z boson into four fermions described by the generic Feynman diagrams shown in Fig. 1. When the exchanged vector bosons are either photons or Z bosons, the four fermion decay contributes at $O(\alpha^2)$. In principle, these decay widths are contained in the Daverveldt Monte Carlo [2,3] which contains a complete description of four fermion production via e^+e^- annihilation. Although the original program [3] contained only the 36 photon exchange graphs, the possibility of exchanging Z bosons has subsequently been included. This program includes all mass effects and the contributions from multiperipheral diagrams in addition to the annihilation diagrams considered here. Up to 144 diagrams contribute to the total $e^+e^- \to f\bar{f}f\bar{f}$ rate and the calculation is only made possible by determining which amplitudes and classes of diagrams may be safely neglected for a given momentum configuration without altering the total cross section. Due to the complexity of the program, it is difficult to extract the contribution from the decay of the Z boson which we are interested in here.

The particularly interesting decay $Z \to q\bar{q}\ell^+\ell^-$ decay has also been studied in Ref. [4]. This decay is interesting because it may provide a background for the discovery of the Higgs boson at LEP or SLC. If the Higgs boson is relatively light, $M_H \lesssim 50$ GeV, it may be copiously produced via the Bjorken process [5],

$$Z \to HZ^* \to Hf\bar{f}, \tag{1.1}$$

which may have a branching rate as large as 10^{-2}. Limits from CUSB [6] and other low energy experiments tend [7] to rule out a Higgs lighter than 3 or 4 GeV, so that the preferred decay modes of the Higgs are $H \to \tau^+\tau^-$, $c\bar{c}$ or $b\bar{b}$. The signal is then typically a quark pair with

invariant mass $m_{q\bar{q}} \sim m_H$ recoiling against the decay products of the virtual Z which tend to be concentrated at large invariant mass, $m_{\ell^+\ell^-} \sim M_Z - m_H$. Although a conclusive analysis of the signal to background ratio requires a full study of the $e^+e^- \to Hf\bar{f} \to f\bar{f}f'\bar{f}'$ and $e^+e^- \to f\bar{f}f'\bar{f}'$ processes, a comparison of the bare Z boson decay suggests [8] that the four fermion decay is not a severe background when the fermions are energetic and well separated.

We organise this paper as follows. In section 2 we use spinor techniques to derive compact analytic expressions for the helicity amplitudes contributing to Z boson decay into four fermions including all mass effects. By constructing generic helicity amplitudes for the exchanged vector bosons, our helicity amplitudes can be applied to both $O(\alpha^2)$ and $O(\alpha_s^2)$ four fermion decay. In the limit of massless fermions, the helicity amplitudes simplify enormously and lead to a fast approximate form for the matrix elements. We then numerically integrate the matrix elements over the four particle phase space to obtain the partial widths. Since there are many singular regions in the phase space, the correct choice of integration variables is important and these are described in section 3. Our numerical results are contained in section 4 where we also make a direct comparison between the four fermion decay and the production and decay of Higgs bosons in Z decay. When the fermions are energetic and well separated, the effect of the fermion mass is rather small and we compare both the massive and massless matrix elements in this region. The decay of the Z boson into four [9,10] and even five [11,12] jets has been studied in the limit of massless partons. Since the partial widths for the $O(\alpha_s^2)$ decay into four massive quarks are easily obtained from the helicity amplitudes presented here, we compute the partial widths for the production of four massive quarks and make a comparison between the massive and massless approximation for the decay of the Z boson into four quarks jets. Finally, in section 5 we summarize our results.

2 Matrix Elements

In this section we present the exact calculation of the matrix elements for the decay of the Z boson into two pairs of massive fermions, f_1 and f_2, of mass m_1 and m_2 respectively,

$$Z \to f_1(p_1) + \bar{f}_1(p_2) + f_2(p_3) + \bar{f}_2(p_4). \tag{2.1}$$

This decay may occur at $O(\alpha^2)$ via photon or Z boson exchange, or, in the case of $Z \to q_1\bar{q}_1q_2\bar{q}_2$, at $O(\alpha_s^2)$ via gluon exchange. Rather than compute the full squared matrix ele-

ments directly for each of these processes, we choose to use a spinor technique to calculate the helicity amplitudes for the generic Feynman diagrams shown in Fig. 1 for the exchange of a vector boson V. The full squared matrix element for a particular process may then be constructed by summing the generic helicity amplitudes over the exchanged vector bosons which contribute and then squaring. Fig. 1b is related to Fig. 1a by the exchange of $f_1 \leftrightarrow f_2$ ($p_1 \leftrightarrow p_3$) and $\bar{f}_1 \leftrightarrow \bar{f}_2$ ($p_2 \leftrightarrow p_4$), while Figs. 1c and 1d only contribute when the fermions are indistinguishable, $f_1 = f_2$, and are obtained by exchanging f_1 and f_2 ($p_1 \leftrightarrow p_3$) in Figs. 1a and 1b. In this case, due to the exchange of anticommuting fermion fields, there is a relative minus sign between the diagrams that ensures that each helicity amplitude vanish when both fermions (antifermions) have identical quantum numbers.

Although the spinor technique of Ref. [13] is extremely convenient for computations involving massless fermions, it is rather more cumbersome when the (anti)fermions are massive. In this method, each massive four vector is written as a sum of two lightlike momenta, and each massive (anti)fermion spinor then expressed as a linear sum of two massless (anti)fermion spinors with opposite helicities. In general, use of this method to describe a system containing four massive fermions would necessitate the introduction of eight massless momenta. However, in the special case where each fermion is accompanied by an antifermion, the two lightlike momenta describing the fermion may also be used to describe the antifermion. For example, we can find lightlike momenta q_1 and q_2 which describe the fermion pair $f_1\bar{f}_1$ with mass m_1 and momenta p_1 and p_2, such that,

$$\left\{ \begin{array}{l} p_1^\mu = x q_1^\mu + y q_2^\mu, \\ \\ p_2^\mu = x q_2^\mu + y q_1^\mu, \end{array} \right\} \leftrightarrow \left\{ \begin{array}{l} q_1^\mu = \frac{x p_1^\mu - y p_2^\mu}{x^2 - y^2}, \\ \\ q_2^\mu = \frac{x p_2^\mu - y p_1^\mu}{x^2 - y^2}, \end{array} \right\}, \tag{2.2}$$

where, since $q_1^2 = q_2^2 = 0$,

$$m_1^2 = p_1^2 = p_2^2 = 2xy(q_1 \cdot q_2). \tag{2.3}$$

The parameters x and y can be covariantly defined in terms of the mass of the p_1p_2 CM system, M_{12}, and the velocity in the CM frame, β_{12},

$$M_{12}^2 = (p_1 + p_2)^2, \qquad \beta_{12} = \sqrt{1 - \frac{4m_1^2}{M_{12}^2}}, \tag{2.4}$$

such that,

$$x = \frac{M_{12}}{4}(1 + \beta_{12}), \qquad y = \frac{M_{12}}{4}(1 - \beta_{12}). \tag{2.5}$$

This corresponds to the choice,

$$(q_1 \cdot q_2) = 2. \tag{2.6}$$

In the limit $m_1 \to 0$, y also tends to zero and q_1 and q_2 become parallel with p_1 and p_2 respectively. In the same way, we may describe the fermion pair $f_2\bar{f}_2$ with mass m_2 and momenta p_3 and p_4 in terms of two lightlike momenta q_3 and q_4,

$$\left\{ \begin{array}{l} p_3^\mu = w q_3^\mu + z q_4^\mu, \\ \\ p_4^\mu = w q_4^\mu + z q_3^\mu, \end{array} \right\} \leftrightarrow \left\{ \begin{array}{l} q_3^\mu = \frac{w p_3^\mu - z p_4^\mu}{w^2 - z^2}, \\ \\ q_4^\mu = \frac{w p_4^\mu - z p_3^\mu}{w^2 - z^2}. \end{array} \right\}. \tag{2.7}$$

w and z are defined in the p_3p_4 CM frame by relations analogous to eqs. (2.4) and (2.5), and, as $m_2 \to 0$, $z \to 0$. In this way the four fermion final state can be described by four lightlike momenta, rather than eight, in a way in which the massless limit is easily taken.

As mentioned above, the spinors of the massive fermions are given by a linear combination of two opposite helicity massless spinors. We use,

$$\bar{u}_+(p_1) = \frac{\sqrt{x}}{2} s_{12}^* \, \bar{u}_+(q_1) + \sqrt{y} \, \bar{u}_-(q_2), \tag{2.8}$$

$$\bar{u}_-(p_1) = \frac{\sqrt{y}}{2} s_{12}^* \, \bar{u}_+(q_2) - \sqrt{x} \, \bar{u}_-(q_1), \tag{2.9}$$

$$u_+(p_2) = -\frac{\sqrt{x}}{2} s_{12} \, u_+(q_2) - \sqrt{y} \, u_-(q_1), \tag{2.10}$$

$$u_-(p_2) = -\frac{\sqrt{y}}{2} s_{12} \, u_+(q_1) + \sqrt{x} \, u_-(q_2). \tag{2.11}$$

The spinor products, s_{ij} and s_{ij}^* are given by,

$$s_{ij} = \bar{u}_+(q_i) u_-(q_j) = -s_{ji}, \tag{2.12}$$

and,

$$s_{ji}^* = \bar{u}_-(q_i) u_+(q_j) = -s_{ij}^*, \tag{2.13}$$

where $u_\pm(q_i)$ denotes the positive (negative)-helicity spinor associated with the lightlike momenta q_i. The absolute square of the spinor product s_{ij} is related to the vector product of q_i and q_j by,

$$|s_{ij}|^2 = 2 \, (q_i \cdot q_j). \tag{2.14}$$

For our choice of q_1 and q_2, $s_{12} = 2 \, e^{i\phi}$, and, in the massless limit ($y \to 0$), the massive and massless spinors are identical up to an overall phase. The spinors describing f_2 and $\bar{f}_2$ are

simply obtained by the replacements,

$$\bar{u}_\lambda(p_3) = \bar{u}_\lambda(p_1)\ \{q_1 \to q_3, q_2 \to q_4, x \to w, y \to z\}, \tag{2.15}$$

$$u_\lambda(p_4) = u_\lambda(p_2)\ \{q_1 \to q_3, q_2 \to q_4, x \to w, y \to z\}. \tag{2.16}$$

A convenient choice for the numerical evaluation of matrix elements expressed in terms of the spinor products is [13],

$$s_{ij} = (q_i^y + iq_i^z)\sqrt{\frac{p_j^0 - p_j^x}{p_i^0 - p_i^x}} - (q_j^y + iq_j^z)\sqrt{\frac{p_i^0 - p_i^x}{p_j^0 - p_j^x}}, \tag{2.17}$$

where,

$$q_i^\mu = (q_i^0, q_i^x, q_i^y, q_i^z). \tag{2.18}$$

The coupling of a vector boson V with fermion $\mathcal{F}_i$ is defined to be,

$$-i(v^{iV} + a^{iV}\gamma_5)\gamma^\mu, \tag{2.19}$$

where v^{iV} and a^{iV} contain the coupling constants and are related to the left- and right-handed couplings by,

$$c_{L,R}^{iV} = v^{iV} \mp a^{iV}. \tag{2.20}$$

In the case of coupling to photons or gluons, the axial coupling a^{iV} is zero and,

$$c_L^{i\gamma} = c_R^{i\gamma}, \qquad c_L^{ig} = c_R^{ig}. \tag{2.21}$$

Finally, the polarization vector of the initial Z boson is described by two more lightlike vectors, q_5 and q_6,

$$\epsilon_\lambda^\mu = \frac{C_\lambda}{M_Z}\ \bar{u}_\lambda(q_5)\gamma^\mu u_\lambda(q_6). \tag{2.22}$$

By making the specific choice,

$$C_{L,R} = \frac{c_{L,R}^{eZ}}{\sqrt{(c_L^{eZ})^2 + (c_R^{eZ})^2}}, \tag{2.23}$$

both the averaging over the spin of the Z boson and any spin correlations arising from the production of the Z boson are automatically included.

2.1 $Z \to f_1 \bar{f}_1 f_2 \bar{f}_2$

We now turn to the helicity amplitudes describing the generic diagrams of Fig. 1a, denoted by,

$$\mathcal{M}^{aV}(\lambda_1, \lambda_2, \lambda_3, \lambda_4; \lambda_5), \tag{2.24}$$

where λ_i $(i = 1, 4)$ is the helicity associated with momenta p_i and λ_5 that associated with momenta q_5 (and q_6). There are four independent amplitudes,

$$\mathcal{M}^{aV}(+,+,+,+;+) = (wc_R^{2V} + zc_L^{2V})\; C_R\; P_{34}^V \times$$
$$\left\{ m_1^2 \left(s_{12} s_{35} s_{24}^* s_{26}^* \left[\frac{c_L^{1Z} c_R^{1V}}{D_1} - \frac{c_R^{1Z} c_L^{1V}}{D_2} \right] - s_{13} s_{15} s_{12}^* s_{46}^* \left[\frac{c_R^{1Z} c_L^{1V}}{D_1} - \frac{c_L^{1Z} c_R^{1V}}{D_2} \right] \right) \right.$$
$$\left. + 4 s_{13} s_{26}^* \left[\frac{x c_R^{1Z} c_R^{1V}}{D_2}\, \mathcal{F}_{12354} - \frac{y c_L^{1Z} c_L^{1V}}{D_1}\, \mathcal{F}_{21354} \right] - 4 s_{15} s_{24}^* \left[\frac{x c_R^{1Z} c_R^{1V}}{D_1}\, \mathcal{F}_{21436} - \frac{y c_L^{1Z} c_L^{1V}}{D_2}\, \mathcal{F}_{12436} \right] \right\}, \tag{2.25}$$

$$\mathcal{M}^{aV}(+,+,+,-;+) = m_2\; C_R\; P_{34}^V \times$$
$$\left\{ \frac{m_1^2 (w+z)^2}{M_V^2} (c_R^{1V} - c_L^{1V})(c_R^{2V} - c_L^{2V}) \times \right.$$
$$\left(s_{15} s_{12}^* (s_{31} s_{36}^* + s_{41} s_{46}^*) \left[\frac{c_R^{1Z}}{D_1} + \frac{c_L^{1Z}}{D_2} \right] - s_{21} s_{26}^* (s_{35} s_{32}^* + s_{45} s_{42}^*) \left[\frac{c_L^{1Z}}{D_1} + \frac{c_R^{1Z}}{D_2} \right] \right)$$
$$+ \frac{m_1^2}{2} s_{15} s_{12}^* \left[c_R^{2V} s_{31} s_{36}^* - c_L^{2V} s_{41} s_{46}^* \right] \left[\frac{c_R^{1Z} c_L^{1V}}{D_1} - \frac{c_L^{1Z} c_R^{1V}}{D_2} \right]$$
$$- \frac{m_1^2}{2} s_{21} s_{26}^* \left[c_R^{2V} s_{35} s_{32}^* - c_L^{2V} s_{45} s_{42}^* \right] \left[\frac{c_R^{1Z} c_L^{1V}}{D_2} - \frac{c_L^{1Z} c_R^{1V}}{D_1} \right]$$
$$+ 2 c_R^{2V} s_{13} s_{26}^* \left[\frac{x c_R^{1Z} c_R^{1V}}{D_2}\, \mathcal{F}_{12453} - \frac{y c_L^{1Z} c_L^{1V}}{D_1}\, \mathcal{F}_{21453} \right] - 2 c_R^{2V} s_{15} s_{23}^* \left[\frac{x c_R^{1Z} c_R^{1V}}{D_1}\, \mathcal{F}_{21436} - \frac{y c_L^{1Z} c_L^{1V}}{D_2}\, \mathcal{F}_{12436} \right]$$
$$\left. + 2 c_L^{2V} s_{15} s_{24}^* \left[\frac{x c_R^{1Z} c_R^{1V}}{D_1}\, \mathcal{F}_{21346} - \frac{y c_L^{1Z} c_L^{1V}}{D_2}\, \mathcal{F}_{12346} \right] - 2 c_L^{2V} s_{14} s_{26}^* \left[\frac{x c_R^{1Z} c_R^{1V}}{D_2}\, \mathcal{F}_{12354} - \frac{y c_L^{1Z} c_L^{1V}}{D_1}\, \mathcal{F}_{21354} \right] \right\}, \tag{2.26}$$

$$\mathcal{M}^{aV}(+,-,+,+;+) = 2\ m_1\ (wc_R^{2V} + zc_L^{2V})\ C_R\ P_{34}^V \times$$

$$\Big\{ + xs_{12}^* s_{46}^* \left[\frac{c_R^{1Z} c_L^{1V}}{D_1} s_{15} s_{23} - \frac{c_L^{1Z} c_R^{1V}}{D_2} s_{13} s_{25}\right] - ys_{12} s_{35} \left[\frac{c_R^{1Z} c_L^{1V}}{D_2} s_{16}^* s_{24}^* - \frac{c_L^{1Z} c_R^{1V}}{D_1} s_{14}^* s_{26}^*\right]$$

$$+ c_R^{1Z} c_R^{1V} \left[\frac{s_{13} s_{16}^*}{D_2}\ \mathcal{F}_{12354} - \frac{s_{15} s_{14}^*}{D_1}\ \mathcal{F}_{21436}\right] + c_L^{1Z} c_L^{1V} \left[\frac{s_{23} s_{26}^*}{D_1}\ \mathcal{F}_{21354} - \frac{s_{25} s_{24}^*}{D_2}\ \mathcal{F}_{12436}\right] \Big\}, \tag{2.27}$$

$$\mathcal{M}^{aV}(+,-,+,-;+) = m_1\ m_2\ C_R\ P_{34}^V \times$$

$$\Big\{ \frac{2(w+z)^2}{M_V^2}\ (c_R^{1V} - c_L^{1V})(c_R^{2V} - c_L^{2V}) \times$$

$$\Big(- \frac{xc_R^{1Z}}{D_1} s_{15} s_{12}^* \left[s_{32} s_{36}^* + s_{42} s_{46}^*\right] + \frac{yc_R^{1Z}}{D_2} s_{12} s_{16}^* \left[s_{35} s_{32}^* + s_{45} s_{42}^*\right]$$

$$+ \frac{xc_L^{1Z}}{D_2} s_{25} s_{21}^* \left[s_{31} s_{36}^* + s_{41} s_{46}^*\right] - \frac{yc_L^{1Z}}{D_1} s_{21} s_{26}^* \left[s_{35} s_{31}^* + s_{45} s_{41}^*\right] \Big)$$

$$- \frac{xc_R^{1Z} c_L^{1V}}{D_1} s_{15} s_{12}^* \left[c_R^{2V} s_{32} s_{36}^* - c_L^{2V} s_{42} s_{46}^*\right] \quad + \frac{yc_R^{1Z} c_L^{1V}}{D_2} s_{12} s_{16}^* \left[c_R^{2V} s_{35} s_{32}^* - c_L^{2V} s_{45} s_{42}^*\right]$$

$$+ \frac{yc_L^{1Z} c_R^{1V}}{D_1} s_{21} s_{26}^* \left[c_R^{2V} s_{35} s_{31}^* - c_L^{2V} s_{45} s_{41}^*\right] \quad - \frac{xc_L^{1Z} c_R^{1V}}{D_2} s_{25} s_{21}^* \left[c_R^{2V} s_{31} s_{36}^* - c_L^{2V} s_{41} s_{46}^*\right]$$

$$+ \frac{c_R^{1Z} c_R^{1V}}{D_1} s_{15} \left[c_L^{2V} s_{14}^*\ \mathcal{F}_{21346} - c_R^{2V} s_{13}^*\ \mathcal{F}_{21436}\right] - \frac{c_R^{1Z} c_R^{1V}}{D_2} s_{16}^* \left[c_L^{2V} s_{14}\ \mathcal{F}_{12354} - c_R^{2V} s_{13}\ \mathcal{F}_{12453}\right]$$

$$+ \frac{c_L^{1Z} c_L^{1V}}{D_2} s_{25} \left[c_L^{2V} s_{24}^*\ \mathcal{F}_{12346} - c_R^{2V} s_{23}^*\ \mathcal{F}_{12436}\right] - \frac{c_L^{1Z} c_L^{1V}}{D_1} s_{26}^* \left[c_L^{2V} s_{24}\ \mathcal{F}_{21354} - c_R^{2V} s_{23}\ \mathcal{F}_{21453}\right] \Big\}. \tag{2.28}$$

The fermion and vector boson propagators are,

$$\begin{aligned} D_i &= \left(\sum_{j=1}^{4} p_j - p_i\right)^2 - m_1^2, \qquad i = 1,2 \\ &= \left(\sum_{j=1}^{4} p_j - p_i\right)^2 - m_2^2, \qquad i = 3,4 \end{aligned} \tag{2.29}$$

and

$$P_{ij}^V = \frac{1}{(p_i + p_j)^2 - M_V^2 + i\Gamma_V M_V}, \tag{2.30}$$

where M_V and Γ_V are the mass and width of the vector boson V. In addition, we have used

the auxiliary function,

$$\mathcal{F}_{ijklm} = x\ s_{il}s^*_{im} + y\ s_{jl}s^*_{jm} + (w+z)\ s_{kl}s^*_{km}. \tag{2.31}$$

The terms proportional to M_V^{-2} come from the $p^\mu p^\nu$ piece of the V propagator. These terms are always multiplied by m_2, which ensures that the axial current is conserved when $m_2 = 0$, and by $(c_R^{2V} - c_L^{2V})$ so that the vector current is conserved for all fermion masses.

The remaining four helicity amplitudes with $\lambda_1 = \lambda_5 = +$ are obtained by the replacements,

$$\mathcal{M}^{aV}(+,\lambda_2,-,-;+) = \mathcal{M}^{aV}(+,\lambda_2,+,+;+)\ \left\{q_3 \leftrightarrow q_4, c_L^{2V} \leftrightarrow c_R^{2V}\right\}, \tag{2.32}$$

$$\mathcal{M}^{aV}(+,\lambda_2,-,+;+) = \mathcal{M}^{aV}(+,\lambda_2,+,-;+)\ \left\{c_L^{2V} \leftrightarrow c_R^{2V}\right\}, \tag{2.33}$$

while the helicity amplitudes with either $\lambda_1 = -$ or $\lambda_5 = -$ are given by,

$$\mathcal{M}^{aV}(-,-\lambda_2,-\lambda_3,-\lambda_4;+) = \mathcal{M}^{*aV}(+,\lambda_2,\lambda_3,\lambda_4;+)\ \left\{q_5 \leftrightarrow q_6, c_L^{iv} \leftrightarrow c_R^{iv}\right\}, \tag{2.34}$$

and,

$$\mathcal{M}^{aV}(\lambda_1,\lambda_2,\lambda_3,\lambda_4;-) = \mathcal{M}^{aV}(\lambda_1,\lambda_2,\lambda_3,\lambda_4;+)\ \{q_5 \leftrightarrow q_6, C_L \leftrightarrow C_R\}, \tag{2.35}$$

where the exchange, $c_L^{iv} \leftrightarrow c_R^{iv}$, is over all fermion couplings $\mathcal{F}_i$ with all vector bosons v.

Finally, the helicity amplitudes for the generic Feynman diagrams shown in Fig. 1b are obtained from $\mathcal{M}^{aV}$ by the permutations,

$$\begin{aligned}&\mathcal{M}^{b\pm}(\lambda_1,\lambda_2,\lambda_3,\lambda_4;\lambda_5) = \\ &\mathcal{M}^{a\pm}(\lambda_3,\lambda_4,\lambda_1,\lambda_2;\lambda_5)\ \left\{q_1 \leftrightarrow q_3, q_2 \leftrightarrow q_4, c_\pm^{1i} \leftrightarrow c_\pm^{2i}, m_1 \leftrightarrow m_2, x \leftrightarrow w, y \leftrightarrow z\right\}.\end{aligned} \tag{2.36}$$

These permutations also imply that $D_1 \leftrightarrow D_3$, $D_2 \leftrightarrow D_4$, $P_{34}^V \leftrightarrow P_{12}^V$ and $\mathcal{F} \leftrightarrow \bar{\mathcal{F}}$ where,

$$\bar{\mathcal{F}}_{ijklm} = \mathcal{F}_{ijklm}\{x \leftrightarrow w, y \leftrightarrow z\}. \tag{2.37}$$

The full helicity amplitude for the decay of the Z boson into two pairs of different fermions is,

$$\mathcal{M}^{ab}_{\lambda_1\lambda_2\lambda_3\lambda_4\lambda_5} = \sum_V\ \mathcal{M}^{aV}(\lambda_1,\lambda_2,\lambda_3,\lambda_4;\lambda_5) + \mathcal{M}^{bV}(\lambda_1,\lambda_2,\lambda_3,\lambda_4;\lambda_5), \tag{2.38}$$

where the sum is over all contributing vector bosons V. The summed and averaged squared matrix elements are obtained by summing squares of the 32 contributing helicity amplitudes,

$$|\mathcal{M}|^2 = C_F \sum_{\lambda_i=\pm,\ i=1,5} \left|\mathcal{M}^{ab}_{\lambda_1\lambda_2\lambda_3\lambda_4\lambda_5}\right|^2, \tag{2.39}$$

where the colour factor C_F depends both on the fermions produced in the decay and the exchanged bosons. For gluon exchange ($Z \to q_1\bar{q}_1q_2\bar{q}_2$) $C_F = 2$, while for γ, Z exchange,

$$C_F = \begin{cases} 1, & Z \to \ell_1\bar{\ell}_1\ell_2\bar{\ell}_2 \\ 3, & Z \to \ell_1\bar{\ell}_1q_2\bar{q}_2 \\ 9, & Z \to q_1\bar{q}_1q_2\bar{q}_2 \end{cases} \tag{2.40}$$

2.2 $Z \to f\bar{f}f\bar{f}$

When the Z boson decays into two pairs of like fermions, the graphs shown in Fig. 1c and 1d also contribute. Although there are some simplifications from the fact that $m_1 = m_2 = m$, $c^{1V}_{L,R} = c^{2V}_{L,R} = c^V_{L,R}$ and $xy = wz$, the particular choice for the physical quark spinors (eqs. (2.8)-(2.11), (2.15) and (2.16)) is not quite as convenient as before. Nevertheless, the generic digrams of Fig. 1c are once again described by four independent helicity amplitudes,

$$\begin{aligned} &\mathcal{M}^{cV}(+,+,+,+;+) = C_R\ P^V_{14}\times \\ &\Bigg\{ + m^2(c^V_R)^2c^Z_L s_{15}s^*_{46}\left[\frac{x}{D_3}s_{43}s^*_{42} - \frac{w}{D_2}s_{13}s^*_{12}\right] + m^2(c^V_L)^2c^Z_R s_{35}s^*_{26}\left[\frac{y}{D_3}s_{31}s^*_{34} - \frac{z}{D_2}s_{21}s^*_{24}\right] \\ &- 4yz(c^V_L)^2c^Z_L\left[\frac{s_{13}s^*_{46}}{D_3}\bar{\mathcal{F}}_{43152} + \frac{s_{15}s^*_{24}}{D_2}\mathcal{F}_{12436}\right] - 4xw(c^V_R)^2c^Z_R\left[\frac{s_{35}s^*_{24}}{D_3}\bar{\mathcal{F}}_{43216} + \frac{s_{13}s^*_{26}}{D_2}\mathcal{F}_{12354}\right] \\ &+ \frac{m^2(c^V_R - c^V_L)^2}{2M^2_V}\ \mathcal{A}_{++}\ \mathcal{B}_{++}\Bigg\}, \end{aligned} \tag{2.41}$$

$$\mathcal{M}^{cV}(+,+,+,-;+) = 2m\ C_R\ P_{14}^V \times$$

$$\Big\{ + yw\frac{(c_L^V)^2 c_R^Z}{D_3} s_{14}s_{35}s_{26}^*s_{34}^* + xz\frac{(c_R^V)^2 c_L^Z}{D_3} s_{15}s_{34}s_{23}^*s_{46}^*$$

$$- xy\frac{(c_L^V)^2 c_R^Z}{D_2} s_{12}s_{45}s_{24}^*s_{26}^* - wz\frac{(c_R^V)^2 c_L^Z}{D_2} s_{13}s_{15}s_{12}^*s_{36}^*$$

$$+ y(c_L^V)^2 c_L^Z \left[\frac{s_{14}s_{46}^*}{D_3}\bar{\mathcal{F}}_{43152} + \frac{s_{15}s_{24}^*}{D_2}\mathcal{F}_{12346}\right] - x(c_R^V)^2 c_R^Z \left[\frac{s_{35}s_{23}^*}{D_3}\bar{\mathcal{F}}_{43216} + \frac{s_{13}s_{26}^*}{D_2}\mathcal{F}_{12453}\right]$$

$$+ \frac{4c_L^V c_R^V (z-w)}{D_2}\left[yc_L^Z + xc_R^Z\right] s_{15}s_{26}^*$$

$$+ \frac{c_L^V c_R^V (w+z)}{D_2}\left[wc_R^Z s_{21}s_{26}^*\left(s_{35}s_{32}^* + s_{45}s_{42}^*\right) - zc_L^Z s_{15}s_{12}^*\left(s_{31}s_{36}^* + s_{41}s_{46}^*\right)\right]$$

$$+ \frac{m(c_R^V - c_L^V)^2}{4M_V^2}\ \mathcal{A}_{++}\ \mathcal{B}_{+-}\Big\}\ , \tag{2.42}$$

$$\mathcal{M}^{cV}(+,-,+,+;+) = 2m\ C_R\ P_{14}^V \times$$

$$\Big\{ + xy\frac{(c_L^V)^2 c_R^Z}{D_3} s_{23}s_{35}s_{26}^*s_{34}^* + wz\frac{(c_R^V)^2 c_L^Z}{D_3} s_{15}s_{34}s_{14}^*s_{46}^*$$

$$+ yz\frac{(c_L^V)^2 c_R^Z}{D_2} s_{12}s_{35}s_{24}^*s_{16}^* + xw\frac{(c_R^V)^2 c_L^Z}{D_2} s_{13}s_{25}s_{12}^*s_{46}^*$$

$$+ z(c_L^V)^2 c_L^Z \left[\frac{s_{23}s_{46}^*}{D_3}\bar{\mathcal{F}}_{43152} + \frac{s_{25}s_{24}^*}{D_2}\mathcal{F}_{12436}\right] - w(c_R^V)^2 c_R^Z \left[\frac{s_{35}s_{14}^*}{D_3}\bar{\mathcal{F}}_{43216} + \frac{s_{13}s_{16}^*}{D_2}\mathcal{F}_{12354}\right]$$

$$+ \frac{4c_L^V c_R^V (y-x)}{D_3}\left[zc_L^Z + wc_R^Z\right] s_{35}s_{46}^*$$

$$+ \frac{c_L^V c_R^V (x+y)}{D_3}\left[xc_L^Z s_{43}s_{46}^*\left(s_{15}s_{14}^* + s_{25}s_{24}^*\right) - yc_R^Z s_{35}s_{34}^*\left(s_{13}s_{16}^* + s_{23}s_{26}^*\right)\right]$$

$$+ \frac{m(c_R^V - c_L^V)^2}{4M_V^2}\ \mathcal{A}_{-+}\ \mathcal{B}_{++}\Big\}\ , \tag{2.43}$$

$$\mathcal{M}^{cV}(+,-,+,-;+) = C_R\ P_{14}^V \times$$

$$\Bigg\{ + \frac{4c_L^V c_R^V (x+y)}{D_3} \left[xz c_L^Z s_{43} s_{46}^* \left(s_{15} s_{13}^* + s_{25} s_{23}^* \right) + yw c_R^Z s_{35} s_{34}^* \left(s_{14} s_{16}^* + s_{24} s_{26}^* \right) \right]$$

$$- \frac{4c_L^V c_R^V (w+z)}{D_2} \left[xz c_L^Z s_{25} s_{21}^* \left(s_{31} s_{36}^* + s_{41} s_{46}^* \right) + yw c_R^Z s_{12} s_{16}^* \left(s_{35} s_{32}^* + s_{45} s_{42}^* \right) \right]$$

$$- wm^2 \frac{(c_L^V)^2 c_R^Z}{D_3} s_{24} s_{35} s_{26}^* s_{34}^* + zm^2 \frac{(c_R^V)^2 c_L^Z}{D_3} s_{15} s_{34} s_{13}^* s_{46}^*$$

$$- ym^2 \frac{(c_L^V)^2 c_R^Z}{D_2} s_{12} s_{45} s_{24}^* s_{16}^* + xm^2 \frac{(c_R^V)^2 c_L^Z}{D_2} s_{13} s_{25} s_{12}^* s_{36}^*$$

$$+ m^2 (c_L^V)^2 c_L^Z \left[\frac{s_{42} s_{46}^*}{D_3} \bar{\mathcal{F}}_{43152} - \frac{s_{25} s_{24}^*}{D_2} \mathcal{F}_{12346} \right] + m^2 (c_R^V)^2 c_R^Z \left[\frac{s_{35} s_{31}^*}{D_3} \bar{\mathcal{F}}_{43216} - \frac{s_{13} s_{16}^*}{D_2} \mathcal{F}_{12453} \right]$$

$$+ 4m^2 c_L^V c_R^V \left(\frac{x-y}{D_3} \left[c_L^Z s_{45} s_{46}^* - c_R^Z s_{35} s_{36}^* \right] + \frac{w-z}{D_2} \left[c_L^Z s_{25} s_{26}^* - c_R^Z s_{15} s_{16}^* \right] \right)$$

$$+ \frac{m^2 (c_R^V - c_L^V)^2}{2M_V^2}\ \mathcal{A}_{-+}\ \mathcal{B}_{+-} \Bigg\}\ . \tag{2.44}$$

The contribution from the $p^\mu p^\nu$ piece of the V propagator is again proportional to $m\,(c_R^V - c_L^V)$ and is given by the functions $\mathcal{A}_{\lambda_2\lambda_3}$ and $\mathcal{B}_{\lambda_1\lambda_4}$,

$$\begin{aligned}
\mathcal{A}_{++} = &+ \sqrt{xz} \frac{c_R^Z}{D_2} s_{12} s_{26}^* \left[x s_{15} s_{14}^* + y s_{25} s_{24}^* + z s_{35} s_{34}^* \right] \\
&+ \sqrt{xz} \frac{c_L^Z}{D_3} s_{12} s_{46}^* \left[x s_{15} s_{12}^* + w s_{45} s_{42}^* + z s_{35} s_{32}^* \right] \\
&+ \sqrt{yw} \frac{c_R^Z}{D_3} s_{35} s_{34}^* \left[y s_{12} s_{62}^* + w s_{14} s_{64}^* + z s_{13} s_{63}^* \right] \\
&+ \sqrt{yw} \frac{c_L^Z}{D_2} s_{15} s_{34}^* \left[x s_{13} s_{16}^* + y s_{23} s_{26}^* + w s_{43} s_{46}^* \right],
\end{aligned} \tag{2.45}$$

$$\begin{aligned}
\mathcal{A}_{-+} = &+ \sqrt{yz} \frac{c_R^Z}{D_2} s_{12} s_{16}^* \left[x s_{15} s_{14}^* + y s_{25} s_{24}^* + z s_{35} s_{34}^* \right] \\
&+ \sqrt{yz} \frac{c_L^Z}{D_3} s_{12} s_{46}^* \left[y s_{25} s_{21}^* + w s_{45} s_{41}^* + z s_{35} s_{31}^* \right] \\
&- \sqrt{xw} \frac{c_R^Z}{D_3} s_{35} s_{34}^* \left[x s_{12} s_{16}^* + w s_{42} s_{46}^* + z s_{32} s_{36}^* \right] \\
&- \sqrt{xw} \frac{c_L^Z}{D_2} s_{25} s_{34}^* \left[x s_{13} s_{16}^* + y s_{23} s_{26}^* + w s_{43} s_{46}^* \right],
\end{aligned} \tag{2.46}$$

and,

$$\begin{aligned} \mathcal{B}_{++} &= -\sqrt{xz}\; s_{13}s_{12}^* - \sqrt{yw}\; s_{34}s_{24}^*, \\ \mathcal{B}_{+-} &= +\sqrt{xw}\; s_{14}s_{12}^* + \sqrt{yz}\; s_{34}s_{32}^*. \end{aligned} \tag{2.47}$$

The other 28 helicity amplitudes are obtained by the simple replacements,

$$\mathcal{M}^{cV}(\lambda_1,\lambda_2,-\lambda_3,-\lambda_4;\lambda_5) = \mathcal{M}^{cV}(\lambda_1,\lambda_2,\lambda_3,\lambda_4;\lambda_5)\ \{q_3 \leftrightarrow q_4, w \leftrightarrow z\}, \tag{2.48}$$

$$\mathcal{M}^{cV}(-\lambda_1,-\lambda_2,\lambda_3,\lambda_4;\lambda_5) = \mathcal{M}^{cV}(\lambda_1,\lambda_2,\lambda_3,\lambda_4;\lambda_5)\ \{q_1 \leftrightarrow q_2, x \leftrightarrow y\}, \tag{2.49}$$

$$\mathcal{M}^{cV}(\lambda_1,\lambda_2,\lambda_3,\lambda_4;-\lambda_5) = \mathcal{M}^{cV}(\lambda_1,\lambda_2,\lambda_3,\lambda_4;\lambda_5)\ \{q_5 \leftrightarrow q_6, C_R \leftrightarrow C_L\}, \tag{2.50}$$

while the helicity amplitudes for final set of diagrams in Fig. 1d are obtained by the permutations,

$$\mathcal{M}^{dV}(\lambda_1,\lambda_2,\lambda_3,\lambda_4;\lambda_5) = \mathcal{M}^{cV}(\lambda_3,\lambda_4,\lambda_1,\lambda_2;\lambda_5)\ \{q_1 \leftrightarrow q_3, q_2 \leftrightarrow q_4, x \leftrightarrow w, y \leftrightarrow z\}, \tag{2.51}$$

where the exchanges,

$$\mathcal{F} \leftrightarrow \bar{\mathcal{F}}, D_1 \leftrightarrow D_3, D_2 \leftrightarrow D_4, \text{ and } P_{14}^V \leftrightarrow P_{32}^V, \tag{2.52}$$

are also implied.

The summed and averaged matrix elements for $Z \to f\bar{f}f\bar{f}$ are given by,

$$|\mathcal{M}|^2 = \frac{C_F}{4} \sum_{\lambda_i=\pm,\ i=1,5} \left\{ \left|\mathcal{M}^{ab}_{\lambda_1\lambda_2\lambda_3\lambda_4\lambda_5}\right|^2 + \left|\mathcal{M}^{cd}_{\lambda_1\lambda_2\lambda_3\lambda_4\lambda_5}\right|^2 - I_F\left(\mathcal{M}^{ab}_{\lambda_1\lambda_2\lambda_3\lambda_4\lambda_5}\mathcal{M}^{*cd}_{\lambda_1\lambda_2\lambda_3\lambda_4\lambda_5} + \mathcal{M}^{*ab}_{\lambda_1\lambda_2\lambda_3\lambda_4\lambda_5}\mathcal{M}^{cd}_{\lambda_1\lambda_2\lambda_3\lambda_4\lambda_5}\right)\right\}, \tag{2.53}$$

where $I_F = 1$ for γ, Z exchange and $I_F = -\frac{1}{3}$ for gluon exchange. The factor 1/4 is the phase space reduction factor for two pairs of identical fermions. As before,

$$\mathcal{M}^{cd}_{\lambda_1\lambda_2\lambda_3\lambda_4\lambda_5} = \sum_V \mathcal{M}^{cV}(\lambda_1,\lambda_2,\lambda_3,\lambda_4;\lambda_5) + \mathcal{M}^{dV}(\lambda_1,\lambda_2,\lambda_3,\lambda_4;\lambda_5). \tag{2.54}$$

To make sure that the interference between the diagrams of Fig. 1a(1b) and Fig. 1c(1d) is included correctly, we have verified numerically that when $p_1 = p_3$ and $p_2 = p_4$, 28 of the 32 helicity amplitudes vanish as required by Fermi statistics.

So far we have implicitly assumed that the exchanged bosons are either a photon and Z or a gluon. In general the amplitudes for colour singlet and colour octet exchange do not

interfere with each other and the total width is just the sum of the $O(\alpha^2)$ and $O(\alpha_s^2)$ pieces. However, for the case of four identical quark production only, the interference is not zero and there is an $O(\alpha\alpha_s)$ contribution. The summed and averaged squared matrix elements for this interference term are given by,

$$|\mathcal{M}|^2 = -\sum_{\lambda_i=\pm,\ i=1,5}\Big\{\mathcal{M}^{ab1}_{\lambda_1\lambda_2\lambda_3\lambda_4\lambda_5}\mathcal{M}^{*cd8}_{\lambda_1\lambda_2\lambda_3\lambda_4\lambda_5}+\mathcal{M}^{*ab1}_{\lambda_1\lambda_2\lambda_3\lambda_4\lambda_5}\mathcal{M}^{cd8}_{\lambda_1\lambda_2\lambda_3\lambda_4\lambda_5} + \mathcal{M}^{ab8}_{\lambda_1\lambda_2\lambda_3\lambda_4\lambda_5}\mathcal{M}^{*cd1}_{\lambda_1\lambda_2\lambda_3\lambda_4\lambda_5}+\mathcal{M}^{*ab8}_{\lambda_1\lambda_2\lambda_3\lambda_4\lambda_5}\mathcal{M}^{cd1}_{\lambda_1\lambda_2\lambda_3\lambda_4\lambda_5}\Big\}, \tag{2.55}$$

where now, $\mathcal{M}^{ij1,8}_{\lambda_1\lambda_2\lambda_3\lambda_4\lambda_5}$ refers to the helicity amplitudes, eqs. (2.38) and (2.54), summed over either colour singlet or colour octet exchange. The colour factor in this case is 4, which cancels the identical particle factor of 1/4, while the minus sign is due to Fermi statistics.

2.3 The Limit Of Massless Fermions

Before leaving the subject of the matrix elements, it is interesting to extract the massless fermion limit, $m_1 = 0$ and $m_2 = 0$. Since helicity is conserved at each vertex for massless fermions, the helicity amplitudes simplify dramatically and,

$$\mathcal{M}^{0aV}(+,+,+,-;+) = \mathcal{M}^{0aV}(+,-,+,+;+) = \mathcal{M}^{0aV}(+,-,+,-;+) = 0, \tag{2.56}$$

while $\mathcal{M}^{0aV}(+,+,+,+;+)$ is given by,

$$\begin{aligned}\mathcal{M}^{0aV}(+,+,+,+;+) &= 4\ x\ w\ c_R^{1Z}c_R^{1V}c_R^{2V}C_R\ P_{34}^V\times\\ &\left\{\frac{s_{13}s_{26}^*}{D_2}\left(x\ s_{15}s_{14}^* + w\ s_{35}s_{34}^*\right) - \frac{s_{15}s_{24}^*}{D_1}\left(x\ s_{23}s_{26}^* + w\ s_{43}s_{46}^*\right)\right\},\end{aligned} \tag{2.57}$$

which, when x and w are reabsorbed into the spinor products gives the usual result [13]. The other seven non-zero helicity amplitudes and the amplitudes describing the graphs of Fig. 1b are obtained by the usual permutations, eqs. (2.32) and (2.34)-(2.36).

The helicity amplitudes for the decay into like fermions also simplify in the massless limit, however, due to our particular choices for the fermion spinors and the permutation symmetry amongst the amplitudes, care must be taken. As in the unlike fermion case, there are eight non-zero helicity amplitudes, such that both $\lambda_1\lambda_4$ and $\lambda_2\lambda_3$ are positive, i.e. no helicity flips

at the vertices. We have,

$$\mathcal{M}^{0cV}(+,+,+,+;+) = C_R\ P_{14}^V \times$$

$$\Big\{ -4yz(c_L^V)^2 c_L^Z \left[\frac{s_{13}s_{46}^*}{D_3}\left(y\ s_{15}s_{12}^* + z\ s_{35}s_{32}^*\right) + \frac{s_{15}s_{24}^*}{D_2}\left(y\ s_{23}s_{26}^* + z\ s_{43}s_{46}^*\right)\right] \tag{2.58}$$

$$-4xw(c_R^V)^2 c_R^Z \left[\frac{s_{35}s_{24}^*}{D_3}\left(x\ s_{21}s_{26}^* + w\ s_{41}s_{46}^*\right) + \frac{s_{13}s_{26}^*}{D_2}\left(x\ s_{15}s_{14}^* + w\ s_{35}s_{34}^*\right)\right]\Big\},$$

and,

$$\mathcal{M}^{0cV}(+,-,-,+;+) = C_R\ P_{14}^V \times$$

$$\Big\{ +\frac{4c_L^V c_R^V}{D_3}\left[x^2 w c_L^Z s_{34}s_{36}^*\left(s_{15}s_{14}^* + s_{25}s_{24}^*\right) + y^2 z c_R^Z s_{45}s_{43}^*\left(s_{13}s_{16}^* + s_{23}s_{26}^*\right)\right] \tag{2.59}$$

$$-\frac{4c_L^V c_R^V}{D_2}\left[xw^2 c_L^Z s_{25}s_{21}^*\left(s_{31}s_{36}^* + s_{41}s_{46}^*\right) + yz^2 c_R^Z s_{12}s_{16}^*\left(s_{35}s_{32}^* + s_{45}s_{42}^*\right)\right]\Big\}.$$

In the massless limit, $y \to 0$ and $z \to 0$ and the terms proportional to y and z in these amplitudes do not contribute. However, the two other nonzero amplitudes with λ_5 positive are obtained by the permutations,

$$\mathcal{M}^{0cV}(-\lambda_1,-\lambda_2,-\lambda_3,-\lambda_4;+) = \mathcal{M}^{0cV}(\lambda_1,\lambda_2,\lambda_3,\lambda_4;+)\{q_1 \leftrightarrow q_2, q_3 \leftrightarrow q_4, x \leftrightarrow y, w \leftrightarrow z\}, \tag{2.60}$$

and these terms do then contribute. Finally, the four non-zero amplitudes with λ_5 negative and the amplitudes describing the diagrams of Fig. 1d in the massless limit are given by the usual permutations, eq. (2.51).

3 Phase Space

Once the matrix elements are known, the total width may be obtained by numerical integration over the four body phase space $dLips(4)$,

$$dLips(4) = \frac{d^3p_1}{(2\pi)^3\ 2E_1}\ \frac{d^3p_2}{(2\pi)^3\ 2E_2}\ \frac{d^3p_3}{(2\pi)^3\ 2E_3}\ \frac{d^3p_4}{(2\pi)^3\ 2E_4}\ \delta^4(p_Z - p_1 - p_2 - p_3 - p_4). \tag{3.1}$$

However, due to the large peaking in the amplitudes, the phase space integral requires extreme care. In the worst case, ($Z \to f\bar{f}f\bar{f}$), there are eight propagators which may

become large in different regions of phase space. In the massless fermion case, these propagators contain the infrared and collinear singularities which cause the total width to diverge in the absence of the $O(\alpha^2)$ radiative corrections. When the fermions are massive, these divergences are softened into mass singularities and lead to large logarithms of the form $\log(M_Z/m_e) \sim 19$. Since the correct choice of integration variables is vital to obtain numerically stable results, we will briefly describe them.

When the Z boson decays into two unlike fermion pairs, there are only six potentially large propagators. The phase space is then divided into two regions,

$$S_{12} > S_{34} \text{ or } S_{12} < S_{34}, \tag{3.2}$$

which are related to each other by the exchange $p_1 \leftrightarrow p_3$, $p_2 \leftrightarrow p_4$ and $m_1 \leftrightarrow m_2$ and where $S_{ij} = (p_i + p_j)^2$ (not to be confused with s_{ij}). Let us assume that $S_{12} < S_{34}$. The worst possible behaviour of the amplitudes in this region is proportional to,

$$\frac{1}{S_{12}\ D_3\ D_4} \propto \frac{1}{S_{12}\ E_{12}} \left[\frac{1}{\frac{M_Z}{2} - E_3} + \frac{1}{\frac{M_Z}{2} - E_4} \right], \tag{3.3}$$

where E_i is the energy of particle i in the Z rest frame and $E_{12} = E_1 + E_2$. The phase space integral may be conveniently expressed in terms of the singular variables S_{12}, E_{12} and E_i,

$$dLips(4) = \frac{1}{2^{14}\pi^8}\ dS_{12}\ d\Omega^*_{12} \sqrt{1 - \frac{4m_1^2}{S_{12}}}\ dE_{12}\ dE_i\ d\Omega_i\ d\phi_i, \tag{3.4}$$

where $i = 3$ or 4. Ω^*_{12} are the angles of $\vec{p}_1$ in the rest frame of $\vec{p}_1 + \vec{p}_2$, while Ω_i are the angles of $\vec{p}_i$, and ϕ_i the angle of $\vec{p}_1 + \vec{p}_2$, around $\vec{p}_i$ in the Z CM frame. The most singular parts of the amplitudes may then be smoothed by a simple change of variables, e.g. $dS_{12}/S_{12} \rightarrow d\log S_{12}$. Although the angular integrals have trivial volumina (4π for $d\Omega^*_{12}$, $d\Omega_i$ and 2π for $d\phi_i$), the limits on E_i are more complicated,

$$E_i \gtrless \frac{1}{2} \left[M_Z - E_{12} \pm \sqrt{E_{12}^2 - S_{12}} \sqrt{1 - \frac{4m_1^2}{M_Z^2 - 2M_Z E_{12} + S_{12}}} \right], \tag{3.5}$$

while the boundaries of the S_{12} and E_{12} integrals depend on the fermion masses;

- $m_2 \leq m_1$;

$$4m_1^2 < S_{12} < \frac{M_Z^2}{4} \quad \text{and} \quad \sqrt{S_{12}} < E_{12} < \frac{M_Z}{2}. \tag{3.6}$$

- $m_1 < m_2 \leq \frac{M_Z}{4}$;

$$4m_1^2 < S_{12} < \frac{M_Z^2}{4} \quad \text{and} \quad \sqrt{S_{12}} < E_{12} < min\left[\frac{M_Z}{2}, \frac{M_Z^2 - 4m_2^2 + S_{12}}{2M_Z}\right]. \tag{3.7}$$

- $\frac{M_Z}{4} < m_2$;

$$4m_1^2 < S_{12} < (M_Z - 2m_2)^2 \quad \text{and} \quad \sqrt{S_{12}} < E_{12} < \frac{M_Z^2 - 4m_2^2 + S_{12}}{2M_Z}. \tag{3.8}$$

The boundary condition $4m_1^2 < S_{12} < M_Z^2/4$ looks somewhat unnatural, however, if $\sqrt{S_{12}} > M_Z/2$ then we cannot have $\sqrt{S_{34}} > M_Z/2$ as well and this implies $S_{12} > S_{34}$ contrary to the initial assumption. To obtain the full phase space, the most efficient way is to choose either S_{12} or S_{34} to be the smaller and then to double the phase space volume to account for the excluded region. Furthermore, by allowing each S_{ij} to be chosen to be small 50% of the time, the Monte Carlo integration acts as an event generator.

The phase space for the decay of the Z boson into two like pairs of fermions is more complicated since both S_{32} and S_{14} might also be small. There is no clean way to divide the phase space into four regions with, for example, $S_{12} < S_{34}$, S_{14} and S_{32} which is necessary to have a numerically stable answer. However, by dividing the phase space into two as for the unequal mass fermions, for example $S_{32} < S_{14}$, and then discarding phase space points where $S_{12} < S_{32}$ or $S_{34} < S_{32}$, the integral may be accurately evaluated. In this case, since only one quarter of phase space is kept, the phase space volume should be multiplied by 4 rather than by 2. As in the previous case, to ensure that all regions are well sampled, one should choose each S_{ij} to be the smallest in 25% of the data points.

4 Numerical Results

Using the matrix elements presented in section 2 and the phase space described in the last section, it is now straightforward to compute the partial widths for the decay of the Z boson into four fermions,

$$\Gamma = \frac{1}{2M_Z} \int |\mathcal{M}|^2 \, dLips(4). \tag{4.1}$$

As already mentioned, the inclusion of the fermion masses leads to a finite result for the partial width by modifying the infrared and collinear divergences to give a mass singularity. The resulting widths are logarithmically dependent on the fermion mass and diverge as $m_f \to 0$. This apparent disaster is rectified when the one and two loop graphs, for example, the two loop vertex correction, which contribute at the same order in perturbation theory are included. The mass singularity is cancelled and the total contribution to the Z width is finite as $m_f \to 0$. We have not attempted to estimate these loop corrections here and we emphasize that the partial widths presented here should not be added directly to the total Z width. On the other hand, realistic estimates for the observable widths may be obtained when the fermions are energetic and well separated.

4.1 The $O(\alpha^2)$ Partial Widths

Let us first turn to the total widths for the $O(\alpha^2)$ four fermion decay which are shown in Tables 1-3 for the three distinct final states, $\ell\bar{\ell}\ell'\bar{\ell}'$, $q\bar{q}\ell\bar{\ell}$ and $q\bar{q}q'\bar{q}'$. Since the decay into two pairs of fermions in the same weak isospin doublet, e.g. $Z \to e^+e^-\nu_e\bar{\nu}_e$, is also mediated by W boson exchange [14] we do not quote results for these decays.

As is clearly seen in Tables 1-3, the largest widths occur when the fermions are as light as possible. This is due to the effects of the mass singularity. The dominant contributions have the following typical event structure; one pair of back-to-back fermions with an invariant mass close to M_Z generated by the decay of the Z boson with one of the fermions accompanied by a second pair of soft fermions arising from the conversion of an almost collinear virtual photon. Lighter fermions allow the virtual photon to be closer to its mass shell and lead to a larger contribution to the width. One exception to this, however, is four neutrino production which is only mediated by Z exchange. Consequently, there are no soft or collinear divergences. The total contribution is,

$$\sum \Gamma(Z \to \nu\bar{\nu}\nu\bar{\nu}) = 19.5 \text{ eV}, \tag{4.2}$$

which is equivalent to increasing the Z width by 1.16×10^{-7} neutrino generations. In fact, the pure Z exchange contributes at the level of a few eV in all decays, and, compared to the pure photon exchange contribution, is negligible.

The results presented here differ by a factor of two from the preliminary results quoted

in Ref. [8], due to a double counting in the phase space. There is also an approximate factor of two difference between Table 2 and Ref. [4], however, the difference is more fundamental in decays involving τ leptons and light quarks. Let us now be more specific and attempt to resolve this difference. To do this, we consider the production of $u\bar{u}$ or $d\bar{d}$ pairs in association with either e^+e^- or $\tau^+\tau^-$. In the case of $q\bar{q}e^+e^-$ production, the electrons originate mainly from the virtual photon ($m_e \ll m_q$) so that $\Gamma \sim (v_q^2 + a_q^2)\, e_q^2$ and,

$$\frac{\Gamma(Z \to u\bar{u}e^+e^-)}{\Gamma(Z \to d\bar{d}e^+e^-)} \sim \frac{v_u^2 + a_u^2}{v_d^2 + a_d^2}\,\frac{e_u^2}{e_d^2} \approx 3.1, \tag{4.3}$$

which is in good agreement with the entries in Table 2. (Since we use $m_u = m_d$, any quark mass effects cancel in the ratio.) In $\tau^+\tau^-$ production, the situation is reversed ($m_\tau \gg m_q$) and the quarks are preferentially produced by the photon. The total width is now proportional to the square of the quark charge, $\Gamma \sim e_q^2$ and,

$$\frac{\Gamma(Z \to u\bar{u}\tau^+\tau^-)}{\Gamma(Z \to d\bar{d}\tau^+\tau^-)} \sim \frac{e_u^2}{e_d^2} = 4. \tag{4.4}$$

Again, this agrees well with the entries in Table 2 and disagrees with Ref. [4] which finds a ratio of only 2.5.

To illustrate the pronounced effects of the fermion mass, we consider the decay $Z \to u\bar{u}\ell^+\ell^-$, where $\ell = e, \mu, \tau$. This covers the three regions $m_e \ll m_u$, $m_\mu \sim m_u$ and $m_\tau \gg m_u$. The invariant mass distributions of the lepton pair, $m_{\ell^+\ell^-}$, and quark pair, $m_{u\bar{u}}$ are shown in Fig. 2. The two distributions are correlated - a small value of $m_{\ell^+\ell^-}$, corresponding to a soft virtual photon, $\gamma^* \to \ell^+\ell^-$, is balanced by a large value of $m_{u\bar{u}}$ arising from $Z \to u\bar{u}\gamma^*$ decay, and vice versa. The small $m_{u\bar{u}}$ ($\gamma^* \to u\bar{u}$) and large $m_{\ell^+\ell^-}$ ($Z \to \ell^+\ell^-\gamma^*$) regions depend only on m_u and are insensitive to the lepton mass. Conversely, the large $m_{u\bar{u}}$ ($Z \to u\bar{u}\gamma^*$) and small $m_{\ell^+\ell^-}$ ($\gamma^* \to \ell^+\ell^-$) regions are extremely dependent on the lepton mass and show the diminishing contribution of the photon pole as m_ℓ increases. Since the bin size (2 GeV) is much larger than the mass of both the muon and electron, the $m_{\ell^+\ell^-}$ distributions for $Z \to u\bar{u}e^+e^-$ and $Z \to u\bar{u}\mu^+\mu^-$ differ only in the first bin, peaking at 1.7 10^{-3} for electrons and 1.9 10^{-4} for muons.

In the same way, the lepton energy spectrum, $d\Gamma/dE_{\ell^+}$, shows the same underlying structure. The large E_{ℓ^+} region is dominated by leptons produced directly by the decaying Z boson and is independent of the lepton mass, while the contribution at low E_{ℓ^+} due mainly

to lepton production from the conversion of a virtual photon drops rapidly with increasing m_ℓ.

It is clear that the dominant part of the four fermion decay width occurs when the fermions are either very soft, $E_f \sim 0$, or when they are not well separated, $\theta_{ff'} \sim 0$. It is precisely these regions which are difficult to observe experimentally. A more relevant experimentally observable quantity, however, is the partial width for the decay of the Z boson into four energetic well-separated fermions. To simulate experimental particle separation requirements we impose a cut on the invariant mass of all fermion pairs, $m_{ff'} > 10$ GeV. For our illustrative case we find,

$$\Gamma(Z \to u\bar{u}e^+e^-) = \Gamma(Z \to u\bar{u}\mu^+\mu^-) \sim \Gamma(Z \to u\bar{u}\tau^+\tau^-) \sim 1.6 \text{ keV}, \tag{4.5}$$

corresponding to a branching ratio of 6.4×10^{-7}. The mass dependent singularities have been removed by the cut on the invariant mass of each fermion pair, and the partial widths are now almost independent of the fermion mass.

In Tables 4-6 we show the $O(\alpha^2)$ contributions to the partial widths for Z boson decay into $\ell^+\ell^-\ell'^+\ell'^-$, $q\bar{q}\ell^+\ell^-$ and $q\bar{q}q'\bar{q}'$ with an invariant mass cut of 10 GeV on each possible pairing of fermions. The results in the massless limit are shown in parentheses. In all cases, even for decays involving b quarks, the massless approximation agrees well with the exact result. The total width for the decay into four 'well separated energetic' leptons is,

$$\sum \Gamma(Z \to \ell\bar{\ell}\ell'\bar{\ell}') \sim 4.4 \text{ keV}, \tag{4.6}$$

while the partial width for the production of a large mass isolated lepton pair accompanied by hadrons is,

$$\sum \Gamma(Z \to \ell\bar{\ell}q\bar{q}) \sim 13.4 \text{ keV}. \tag{4.7}$$

These widths correspond to branching ratios of 1.7×10^{-6} and 5.3×10^{-6} respectively, and should easily be within the range of experiments at LEP. Finally, the $O(\alpha^2)$ contribution to Z decay into four 'well separated quark jets' is 8.3 keV. Although this leads to an observable rate, it is swamped by the $O(\alpha_s^2)$ decay into four quarks which we will discuss in section 4.3, and the even more important $Z \to q\bar{q}gg$ decay.

Not only is the total rate independent of the fermion mass, but the invariant mass and energy distributions for the three $Z \to u\bar{u}\ell^+\ell^-$ decays, shown in Figs. 4 and 5, are extremely

similar. In fact, the distributions for $\ell = e$ and $\ell = \mu$ are identical within the statistics of the Monte Carlo, and we show one curve for $\ell = e = \mu$. A small effect due to the mass of the τ is visible at small $m_{\ell^+\ell^-}$ (and hence large $m_{u\bar{u}}$ and small E_{ℓ^+}. This effect is now at the few percent level. There is still a peaking towards small invariant masses due to the photon pole, however, the peak in the lepton energy distribution has been completely removed. Furthermore, the small differences between the $m_{\ell^+\ell^-}$ and $m_{u\bar{u}}$ distributions are due more to the different couplings of the up quark and charged leptons with the Z than the difference in mass. In fact, since the mass dependence has been almost totally removed, taking the limit of massless fermions should be a good approximation. In Figs. 4 and 5, we also show the massless approximation to the partial width. Within the Monte Carlo statistics no difference between the massless case and the results for $l = e$ and $l = \mu$ can be observed. This test provides both a check on the full calculation and a much faster way of estimating the partial width.

4.2 $Z \to H\mu^+\mu^- \to f\bar{f}\mu^+\mu^-$

One practical application of the four fermion decay is in evaluating the background to Higgs production at the Z resonance. As mentioned earlier, due to the large HZZ coupling, the branching rate for the Bjorken process [5] of eq. (1.1) may be as large as 10^{-2}. The Higgs boson then decays preferentially into the heaviest allowed fermion pair, namely $H \to b\bar{b}$, $c\bar{c}$ and $\tau^+\tau^-$, leading to a final state containing four fermions. In this section we compare the two decays specifically for the case when the virtual Z boson decays into a muon pair, $Z^* \to \mu^+\mu^-$, and, since it is difficult to efficiently distinguish quark jets of different flavours, we sum over all possible quarks, $Z \to q\bar{q}\mu^+\mu^-$.

Although the total rates are comparable, the two mechanisms lead to rather different distributions in both $m_{\mu\mu}$ and $m_{q\bar{q}}$ as shown in Figs. 6 and 7. The muons from the virtual Z in the $Z \to H\mu^+\mu^-$ decay have an invariant mass peaked as close to M_Z as possible, while the muons produced in the $Z \to q\bar{q}\mu^+\mu^-$ decay are peaked at both small and large invariant mass reflecting the two contributions from $\gamma^* \to \mu^+\mu^-$ and $Z \to \mu^+\mu^-\gamma^*$. The dominant part of the background is at small invariant mass and is easily removed by a cut on the lepton pair invariant mass. As can be immediately seen from Fig. 6, the four fermion decay of the Z boson does not provide a serious background for Higgs bosons with mass $m_H \leq 45$

GeV.

The invariant mass of the quark pair is, in principle, an accurately measurable quantity since, by momentum conservation, it can be determined directly from the lepton momenta,

$$m_{q\bar{q}}^2 = M_Z^2 - 2M_Z(E_{\mu^+} + E_{\mu^-}) + m_{\mu^+\mu^-}^2. \tag{4.8}$$

The experimental resolution on the invariant mass of the quark pair is therefore determined by how accurately the lepton momenta are measured, and, when the leptons are energetic (which is the case when the Higgs boson is light) the resolution on $m_{q\bar{q}}$ may be quite poor. The two processes lead to quite different $m_{q\bar{q}}$ distributions: The quarks from the Higgs decay have an invariant mass peaked at m_H, while those from the four fermion decay exhibit a similar structure to the $m_{\mu^+\mu^-}$ distribution. Fig. 7 shows the $m_{q\bar{q}}$ distribution assuming a resolution of 2 GeV. With this resolution, the signal clearly stands above the background provided $m_H \leq 45$ GeV. However, by making a cut on the invariant mass of the lepton pair, $m_{\mu^+\mu^-} > 20$ GeV, the background is reduced by well over an order of magnitude at large $m_{q\bar{q}}$, while the signal is almost unaffected. This is summarised in Table 7, where we give the number of events from both the signal and the background per GeV of resolution for a data sample of 10^7 Z events. Since the width of the Higgs boson is very small, $\Gamma_H \sim 2$ MeV for $m_H = 50$ GeV, the signal events all populate one bin. The number of background events, however, is obtained by integrating $d\Gamma(Z \to q\bar{q}\mu^+\mu^-)/dm_{q\bar{q}}$ over a range of $m_{q\bar{q}}$ which depends on the experimental resolution. The signal clearly dominates provided the resolution is less than a few GeV, and the four fermion decay is therefore not a severe background to Higgs detection in Z decay.

4.3 The $O(\alpha_s^2)$ Partial Widths

Approximately 70% of Z bosons decay hadronically, and therefore provide a good testing ground for QCD. The strong interaction is important both in radiatively correcting the total Z width and in introducing new decay topologies. The full $O(\alpha_s^2)$ corrections to the Z width have recently been computed [15] and lead to an increase in Γ_Z of about 5 MeV, which is to be compared with the more important $O(\alpha_s)$ contribution [16] of about 90 MeV. Meanwhile, the exact leading order QCD matrix elements for four jet [9,10] and five jet [11,12] decay have also been computed in the limit of massless partons. In this section we give the (finite)

results for the production of four massive quarks at $O(\alpha_s^2)$ and make some comparisons with the massless case.

The partial widths are shown in Table 8 where we have taken $m_u = m_d = m_s = 0.3$ GeV which represents a typical hadronic mass scale, $m_c = 1.5$ GeV and $m_b = 4.5$ GeV. We have taken the running strong coupling constant to be, $\alpha_s(M_Z^2) = 0.11$ which is the value extracted from determinations of $\alpha_s(Q^2)$ at lower Q^2 [17]. Due to the fact that the exchanged gluon is massless, the partial widths increase with decreasing quark masses. Since QCD is flavour blind, we find,

$$\frac{\Gamma(Z \to u\bar{u}s\bar{s})}{\Gamma(Z \to d\bar{d}s\bar{s})} \sim \frac{v_u^2 + a_u^2 + v_s^2 + a_s^2}{v_d^2 + a_d^2 + v_s^2 + a_s^2} = 0.89, \tag{4.9}$$

where all mass effects have cancelled in the ratio, and which agrees well with Table 8. Furthermore the widths for the production of a heavy quark with any light quark are approximately equal,

$$\Gamma(Z \to Q\bar{Q}u\bar{u}) \sim \Gamma(Z \to Q\bar{Q}d\bar{d}) = \Gamma(Z \to Q\bar{Q}s\bar{s}), \tag{4.10}$$

which is in good agreement with Table 8 for both c and b quarks. For identical light quark production, there is little interference between the contributions from Figs. 1a,b and Figs. 1c,d due to the rather distinct kinematic configurations of the dominant regions of phase space and the following relations are also obeyed,

$$\frac{\Gamma(Z \to u\bar{u}u\bar{u})}{\Gamma(Z \to u\bar{u}d\bar{d})} \sim \frac{v_u^2 + a_u^2}{v_u^2 + a_u^2 + v_d^2 + a_d^2} = 0.44, \tag{4.11}$$

and,

$$\frac{\Gamma(Z \to d\bar{d}d\bar{d})}{\Gamma(Z \to d\bar{d}s\bar{s})} = 0.50. \tag{4.12}$$

In both cases, the entries in Table 8 are slightly smaller reflecting the destructive interference caused by the colour factor, $Tr(T^aT^bT^aT^b) = -\frac{2}{3}$, between the two sets of diagrams. This contrasts with the $O(\alpha^2)$ process where there is a slight constructive interference.

One sees that the total contribution is around 130 MeV (in contrast to the $O(\alpha^2)$ contribution of only 0.17 MeV), which reflects the fact that we have not considered the loop diagrams which also contribute at $O(\alpha_s^2)$. These virtual corrections cancel the mass singularities and reduce the contribution to the full width. On the other hand, the four b quark final state, $Z \to b\bar{b}b\bar{b}$, is in principle completely identifiable since the decay products of soft b quarks can be detected. For a data sample of 10^7 Z decays, there will be approximately

1400 events containing four b quarks. One can apply similar arguments for decays involving c quarks, yielding 6300 $c\bar{c}c\bar{c}$ events and 9400 $c\bar{c}b\bar{b}$ events in the same data sample.

The light quarks, however, are not directly identifiable and appear as jets of hadrons. Two frequently used methods to define jets are using either the Sterman-Weinberg jet resolution parameters ϵ and δ [18], or by imposing a minimum invariant mass on each parton pair,

$$\frac{(p_i + p_j)^2}{M_Z^2} > y_{min}. \tag{4.13}$$

Both methods have been used in lower energy e^+e^- experiments and agree well with the data [19]. In Fig. 8 we show the y_{min} distribution both summed over all quarks and for the $b\bar{b}b\bar{b}$ final state. The rapid growth as $y_{min} \to 0$ reflects the mass singularity once more, and, in the limit $m_q \to 0$ would diverge. The $b\bar{b}b\bar{b}$ contribution, however, vanishes at $y_{min} \sim 0.01$ due to threshold effects. For comparison, we also show in Fig. 8 the result for massless quarks where we have imposed the cutoff $m_{ff'} > 10$ GeV. Unsurprisingly, the distribution summed over all quarks is well described by the massless result, while the $b\bar{b}b\bar{b}$ distribution is slightly harder than in the massless limit.

As mentioned in section 2, there is an $O(\alpha\alpha_s)$ contribution to the Z decay width into four identical quarks, which is suppressed by $O(\alpha/\alpha_s)$ relative to the $O(\alpha_s^2)$ partial widths. Furthermore, since this contribution arises solely from the already small cross terms, there is a further suppression. We find,

$$\begin{aligned} \Gamma(Z \to u\bar{u}u\bar{u}) &= 55 \text{ keV}, \\ \Gamma(Z \to d\bar{d}d\bar{d}) &= 17 \text{ keV}, \\ \Gamma(Z \to c\bar{c}c\bar{c}) &= 24 \text{ keV}, \\ \Gamma(Z \to b\bar{b}b\bar{b}) &= 1.2 \text{ keV}, \end{aligned} \tag{4.14}$$

while the $\Gamma(Z \to s\bar{s}s\bar{s})$ partial width is identical to that for the decay into four d quarks. These widths, which are large compared to the $O(\alpha^2)$ partial widths are nevertheless still very small, $\sim 1\%$, compared to the $O(\alpha_s^2)$ contribution.

As a final comment, let us note that although the $Z \to q\bar{q}q\bar{q}$ rate is quite large, $\Gamma \sim 3$ MeV for $y_{min} > 0.02$, compared to the full $O(\alpha_s^2)$ contribution of 5 MeV, the $Z \to q\bar{q}gg$ rate is

much larger [9,10].

5 Conclusions

In conclusion, we have studied the four fermion decay of the Z boson keeping all dependence on the fermion masses and have presented some numerical results for both the $O(\alpha^2)$ and $O(\alpha_s^2)$ decay. These decay widths, which are finite when integrated over all phase space, were computed using the helicity amplitudes presented in section 2. However, the partial widths are logarithmically dependent on the fermion mass, and, in the absence of the one and two loop radiative corrections that contribute at the same order in perturbation series, should not be directly added to the total Z width.

On the other hand, distinct event topologies may occur, for example, four lepton events, or lepton pairs recoiling against one or two hadronic jets. In these cases, the energy/momentum and separation criteria necessary to experimentally identify the final state, dramatically reduce the observable branching fraction. We have attempted to simulate realistic detector requirements by requiring that all pairs of fermions have an invariant mass, $m_{ff'} > 10$ GeV. In this case, the effect of the fermion mass is much reduced and the full massive matrix elements are well approximated by the massless matrix elements also given in section 2. Typical branching ratios for the decay into four 'well separated energetic' fermions are $Br(Z \to \ell^+\ell^-\ell'^+\ell'^-) \sim 1.7 \times 10^{-6}$ and $Br(Z \to \ell^+\ell^- q\bar{q}) \sim 5.3 \times 10^{-6}$ and which are well within the range of experiments at LEP.

Another source of four fermion events is the production and decay of the Higgs boson via the Bjorken mechanism. We have made a direct comparison between the Higgs boson signal and the four fermion decay and find that, due to the rather different topologies, the background may be easily suppressed by making an invariant mass cut on the lepton pair, leaving a clear Higgs boson signal which is only limited by the integrated luminosity. Given 10^7 Z boson events, the Higgs boson may be clearly seen above the four fermion background for $m_H \leq 60$ GeV.

We have also presented estimates for the $O(\alpha_s^2)$ four quark jet final state, although in this case, the dominant contribution to four jet events is $Z \to q\bar{q}gg$. Once again, the massless

matrix elements are a good description of the full massive matrix elements for reasonable jet definition criteria. Finally, we found a significant branching fraction rate for Z boson decay into four heavy quarks,

$$\frac{\Gamma_{c\bar{c}c\bar{c}}}{\Gamma_{c\bar{c}}} \sim 5.3 \times 10^{-3}, \tag{5.1}$$

$$\frac{\Gamma_{b\bar{b}c\bar{c}}}{\Gamma_{b\bar{b}}} \sim 6.3 \times 10^{-3}, \tag{5.2}$$

and,

$$\frac{\Gamma_{b\bar{b}b\bar{b}}}{\Gamma_{b\bar{b}}} \sim 9.1 \times 10^{-4}. \tag{5.3}$$

Acknowledgements

We would like to thank G. Altarelli for useful discussions.

References

[1] D. Decamp *et al*, ALEPH Collaboration, CERN preprint CERN-EP/89-132 (1989);
P. Aarnio *et al*, DELPHI Collaboration, CERN preprint CERN-EP/89-134 (1989);
B. Adeva *et al*, L3 Collaboration, Preprint L3-001 (1989);
M. Z. Akrawy *et al*, OPAL Collaboration, CERN preprint CERN-EP/89-133 (1989).

[2] F. A. Berends, P. H. Daverveldt and R. Kleiss, Comp. Phys. Comm. **40**, 285 (1986); Comp. Phys. Comm. **40**, 309 (1986).

[3] F. A. Berends, P. H. Daverveldt and R. Kleiss, Phys. Lett. **148B**, 489 (1984); Nucl. Phys. **253**, 441 (1985).

[4] P. Kalyniak, J. N. Ng, and P. Zakarauskas, Phys. Rev. **D30**, 123 (1984).

[5] J. D. Bjorken, in *Weak Interactions at High Energy and the Production of New Particles*, Proceedings of the SLAC Summer Institute on Particle Physics, 1976, edited by M. Zipf, p1 (1976).

[6] J. Lee-Franzini, CUSB Collaboration, invited talk in *Proceedings of the XXIVth International Conference on High Energy Physics*, Munich, Germany, 1988.

[7] For a review of the limits on light Higgs bosons, see, for example, M. Drees *et al* CERN preprint CERN-TH.5487/89 (1989).

[8] W. Bernreuther *et al*, CERN preprint CERN-TH.5484/89 (1989).

[9] A. Ali *et al.*, Phys. Lett. **82B**, 285 (1979); Nucl. Phys. **B167**, 454 (1980).

[10] R. K. Ellis, D. A. Ross and A. E. Terrano, Phys. Rev. Lett. **45**, 1226 (1980); Nucl. Phys. **178**, 421 (1981).

[11] F. A. Berends, W. T. Giele and H. Kuijf, Nucl. Phys. **321**, 39 (1989).

[12] N. K. Falck, D. Graudenz and G. Kramer, Phys. Lett. **220B**, 299 (1989).

[13] R. Kleiss and W. J. Stirling, Nucl. Phys. **B262**, 235 (1985).

[14] W. J. Marciano and D. Wyler, Z. Phys. **C3**, 181 (1979).

[15] B. A. Kniehl and J. H. Kühn, Phys. Lett. **B224**, 229 (1989) and Max Planck preprint MPI-PAE/Pth 39/89.

[16] K. G. Chetrykin *et al.*, Phys. Lett. **85B**, 277 (1979);
M. Dine *et al.*, Phys. Rev. Lett. **43**, 668 (1979);
W. Celmaster *et al.*, Phys. Rev. Lett. **44**, 560 (1979).

[17] G. Altarelli, CERN-TH-5290/89 (1989).

[18] G. Sterman and S. Weinberg, Phys. Rev. Lett. **39**, 1436 (1977).

[19] W. Bartel *et al.*, JADE Collaboration, Z. Phys. **C33**, 23 (1986).

Table 1

The $O(\alpha^2)$ partial width for the decay $Z \to \ell\bar{\ell}\ell'\bar{\ell}'$ in MeV. For the numerical results we have taken $M_Z = 91.1$ GeV in accordance with the latest results from LEP and SLC, while the Weinberg angle is defined in terms of the Fermi constant and the running electric coupling constant, $\alpha(M_Z)$, yielding $\sin^2\theta_W = 0.23$.

$Z \to \ell\bar{\ell}\ell'\bar{\ell}'$	e^+e^-	$\mu^+\mu^-$	$\tau^+\tau^-$	$\nu_e\bar{\nu}_e$	$\nu_\mu\bar{\nu}_\mu$
e^+e^-	0.27	0.28	0.17	-	$6.5 \cdot 10^{-6}$
$\mu^+\mu^-$	0.28	0.033	0.031	$6.5 \cdot 10^{-6}$	-
$\tau^+\tau^-$	0.17	0.031	0.0032	$6.5 \cdot 10^{-6}$	$6.5 \cdot 10^{-6}$
$\nu_e\bar{\nu}_e$	-	$6.5 \cdot 10^{-6}$	$6.5 \cdot 10^{-6}$	$3.1 \cdot 10^{-6}$	$3.4 \cdot 10^{-6}$
$\nu_\mu\bar{\nu}_\mu$	$6.5 \cdot 10^{-6}$	-	$6.5 \cdot 10^{-6}$	$3.4 \cdot 10^{-6}$	$3.1 \cdot 10^{-6}$

Table 2

The $O(\alpha^2)$ partial width for the decay $Z \to \ell\ell q\bar{q}$ in MeV. For the light quark masses we choose, $m_u = m_d = m_s = 0.3$ GeV, which represents the typical hadronic mass scale, while for the heavy quarks, we take, $m_c = 1.5$ GeV and $m_b = 4.5$ GeV.

$Z \to q\bar{q}\ell\bar{\ell}$	$u\bar{u}$	$d\bar{d}$	$s\bar{s}$	$c\bar{c}$	$b\bar{b}$
e^+e^-	0.37	0.12	0.12	0.29	0.07
$\mu^+\mu^-$	0.07	0.021	0.021	0.048	0.012
$\tau^+\tau^-$	0.026	0.007	0.007	0.010	0.0015
$\nu\bar{\nu}$	$5.5 \cdot 10^{-6}$	$41 \cdot 10^{-6}$	$41 \cdot 10^{-6}$	$5.5 \cdot 10^{-6}$	$38 \cdot 10^{-6}$

Table 3

The $O(\alpha^2)$ partial width for the decay $Z \to q\bar{q}q'\bar{q}'$ in MeV. For the light quark masses we choose, $m_u = m_d = m_s = 0.3$ GeV, which represents the typical hadronic mass scale, while for the heavy quarks, we take, $m_c = 1.5$ GeV and $m_b = 4.5$ GeV.

$Z \to q\bar{q}q'\bar{q}'$	$u\bar{u}$	$d\bar{d}$	$s\bar{s}$	$c\bar{c}$	$b\bar{b}$
$u\bar{u}$	0.034	-	0.019	0.039	0.009
$d\bar{d}$	-	0.0028	0.0055	0.010	0.0022
$s\bar{s}$	0.019	0.0055	0.0028	-	0.0022
$c\bar{c}$	0.039	0.010	-	0.008	0.0026
$b\bar{b}$	0.009	0.0022	0.0022	0.0026	0.0001

Table 4

The $O(\alpha^2)$ partial width for the decay $Z \to \ell^+\ell^-\ell'^+\ell'^-$ in keV with an invariant mass cut on each fermion pair, $m_{ff'} > 10$ GeV. The figures in parentheses are the results from making the approximation that the fermions are massless.

$Z \to \ell\bar{\ell}\ell'\bar{\ell}'$	e^+e^-	$\mu^+\mu^-$	$\tau^+\tau^-$
e^+e^-	0.53 (0.54)	0.90 (0.90)	0.95 (0.90)
$\mu^+\mu^-$	0.90 (0.90)	0.52 (0.54)	0.95 (0.90)
$\tau^+\tau^-$	0.95 (0.90)	0.95 (0.90)	0.59 (0.54)

Table 5

The $O(\alpha^2)$ partial width for the decay $Z \to \ell^+\ell^- q\bar{q}$ in keV where an invariant mass cut on each fermion pair of $m_{ff'} > 10$ GeV has been imposed. The figures in parentheses are the partial widths obtained in the limit of massless fermions.

$Z \to q\bar{q}\ell\bar{\ell}$	$u\bar{u}$	$d\bar{d}$	$s\bar{s}$	$c\bar{c}$	$b\bar{b}$
e^+e^-	1.6 (1.6)	0.38 (0.38)	0.38 (0.38)	1.6 (1.6)	0.42 (0.38)
$\mu^+\mu^-$	1.6 (1.6)	0.38 (0.38)	0.38 (0.38)	1.62 (1.6)	0.43 (0.38)
$\tau^+\tau^-$	1.67 (1.6)	0.40 (0.38)	0.40 (0.38)	1.69 (1.6)	0.45 (0.38)

Table 6

The $O(\alpha^2)$ partial width for the decay $Z \to q\bar{q}q'\bar{q}'$ in keV. All pairs of fermions are required to have an invariant mass, $m_{ff'} > 10$ GeV. The figures in parentheses are the partial widths obtained in the limit of massless fermions.

$Z \to q\bar{q}q'\bar{q}'$	$u\bar{u}$	$d\bar{d}$	$s\bar{s}$	$c\bar{c}$	$b\bar{b}$
$u\bar{u}$	1.1 (1.1)	-	0.58 (0.58)	1.9 (1.9)	0.64 (0.58)
$d\bar{d}$	-	0.078 (0.078)	0.15 (0.15)	0.60 (0.58)	0.17 (0.15)
$s\bar{s}$	0.58 (0.58)	0.15 (0.15)	0.078 (0.078)	-	0.17 (0.15)
$c\bar{c}$	1.9 (1.9)	0.60 (0.58)	-	1.18 (1.1)	0.66 (0.58)
$b\bar{b}$	0.64 (0.58)	0.17 (0.15)	0.17 (0.15)	0.66 (0.58)	0.094 (0.078)

Table 7

The number of $q\bar{q}\mu^+\mu^-$ events from both the signal, $Z \to H\mu^+\mu^- \to q\bar{q}\mu^+\mu^-$ with the branching ratio for Higgs decay into c and b quark pairs folded in and the background per GeV of resolution for a data sample of 10^7 Z bosons ($\int \mathcal{L}dt \sim 250$ pb^{-1}). The effect of the $m_{\mu^+\mu^-}$ cut on the signal is shown in brackets.

		$Z \to q\bar{q}\mu^+\mu^-$	
m_H (GeV)	$Z \to H\mu^+\mu^- \to q\bar{q}\mu^+\mu^-$	no cut	$m_{\mu^+\mu^-} > 20$ GeV
5	1017 (1011)	8.2	8.0
15	408 (403)	1.2	0.79
25	168 (163)	0.94	0.19
35	67 (64)	1.5	0.097
45	24 (21)	2.1	0.084
55	7.1 (5.4)	3.5	0.075
65	1.4 (0.6)	5.5	0.043

Table 8

The $O(\alpha_s^2)$ partial width for the decay $Z \to q\bar{q}q'\bar{q}'$ in MeV. For the light quark masses we choose, $m_u = m_d = m_s = 0.3$ GeV, which represents the typical hadronic mass scale, while for the heavy quarks, we take, $m_c = 1.5$ GeV and $m_b = 4.5$ GeV. The strong running coupling constant is $\alpha_s(M_Z^2) = 0.11$.

$Z \to q\bar{q}q'\bar{q}'$	$u\bar{u}$	$d\bar{d}$	$s\bar{s}$	$c\bar{c}$	$b\bar{b}$
$u\bar{u}$	7.0	16.8	16.8	8.7	8.0
$d\bar{d}$	16.8	9.3	19.2	9.1	7.9
$s\bar{s}$	16.8	19.2	9.3	9.1	7.9
$c\bar{c}$	8.7	9.1	9.1	1.6	2.4
$b\bar{b}$	8.0	7.9	7.9	2.4	0.35

Figure Captions

Fig. 1: The Feynman diagrams for the decay $Z \to f_1\bar{f}_1 f_2\bar{f}_2$ mediated by the exchange of vector boson V.

Fig. 2: The invariant mass distribution of (a) the lepton pair, $d\Gamma/dm_{\ell^+\ell^-}$ and (b) the up quark pair, $d\Gamma/dm_{u\bar{u}}$, for the decay $Z \to u\bar{u}\ell^+\ell^-$ where $\ell = e$, μ and τ.

Fig. 3: The lepton energy distribution $d\Gamma/dE_{\ell^+}$ for the decay $Z \to u\bar{u}\ell^+\ell^-$ where $\ell = e$, μ and τ.

Fig. 4: The invariant mass distribution of (a) the lepton pair, $d\Gamma/dm_{\ell^+\ell^-}$ and (b) the up quark pair, $d\Gamma/dm_{u\bar{u}}$, for the decay $Z \to u\bar{u}\ell^+\ell^-$ where $\ell = e = \mu$ and $\ell = \tau$ with an invariant mass cut on all possible fermion pairs, $m_{ff'} > 10$ GeV. The approximate distribution resulting from the use of the massless matrix elements is shown crossed.

Fig. 5: The lepton energy distribution $d\Gamma/dE_{\ell^+}$ for the decay $Z \to u\bar{u}\ell^+\ell^-$ where $\ell = e = \mu$ and $\ell = \tau$ with an invariant mass cut on all possible fermion pairs, $m_{ff'} > 10$ GeV. The approximate distribution resulting from the use of the massless matrix elements is shown crossed.

Fig. 6: The invariant mass distribution of the muon pair, $d\Gamma/dm_{\mu^+\mu^-}$, produced in both $Z \to q\bar{q}\mu^+\mu^-$ decay and $Z \to H\mu^+\mu^- \to q\bar{q}\mu^+\mu^-$ decay for $m_H = 5$, 15, 25, 35, 45, 55 and 65 GeV. The branching ratio for Higgs decay into heavy quarks, $H \to b\bar{b}$ and $H \to c\bar{c}$, has been folded into the signal, while the background is summed over all quark flavours. The contribution from $Z \to b\bar{b}\mu^+\mu^-$ is shown separately.

Fig. 7: The invariant mass distribution of the quark pair, $d\Gamma/dm_{q\bar{q}}$ produced in both $Z \to q\bar{q}\mu^+\mu^-$ decay and $Z \to H\mu^+\mu^- \to q\bar{q}\mu^+\mu^-$ decay for $m_H = 5$, 15, 25, 35, 45, 55 and 65 GeV. Both $H \to b\bar{b}$ and $H \to c\bar{c}$ decays are included in the signal, while the background is summed over all quark flavours. We also show the effect of making a cut on the invariant mass of the muon pair, $m_{\mu^+\mu^-} > 20$ GeV.

Fig. 8: The y_{min} distribution, $d\Gamma/dy_{min}$, for the $O(\alpha_s^2)$ $Z \to q\bar{q}q\bar{q}$ decay summed over all combinations of quarks where y_{min} is defined as the minimum value of $\frac{m^2_{qq'}}{M_Z^2}$. The contribution from $Z \to b\bar{b}b\bar{b}$ is shown separately. As a comparison, we also show,

as crosses, the distributions obtained using the massless matrix elements where we have imposed the invariant mass cut, $m_{ff'} > 10$ GeV on all quark pairs.

Fig. 1

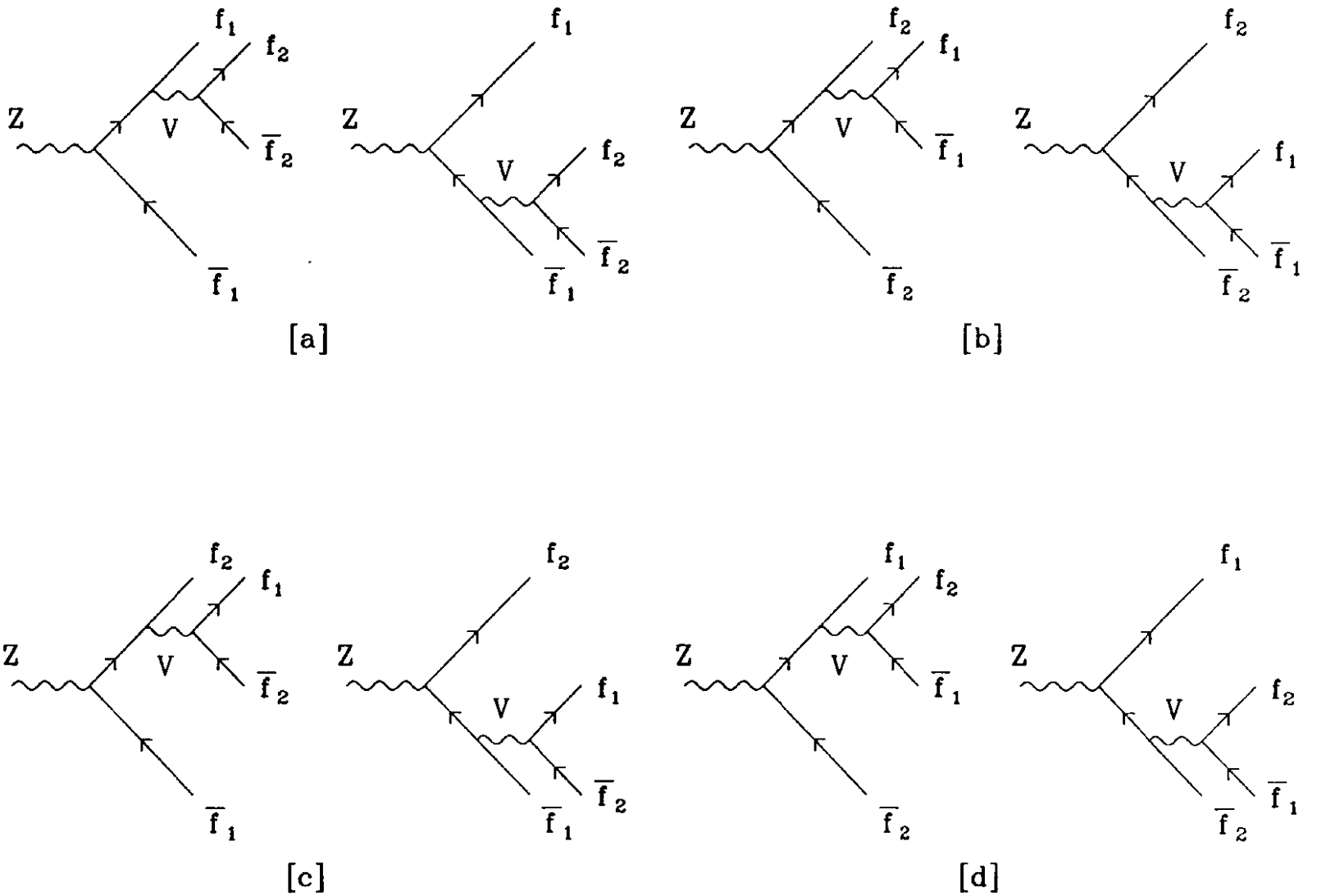

Fig. 2(a)

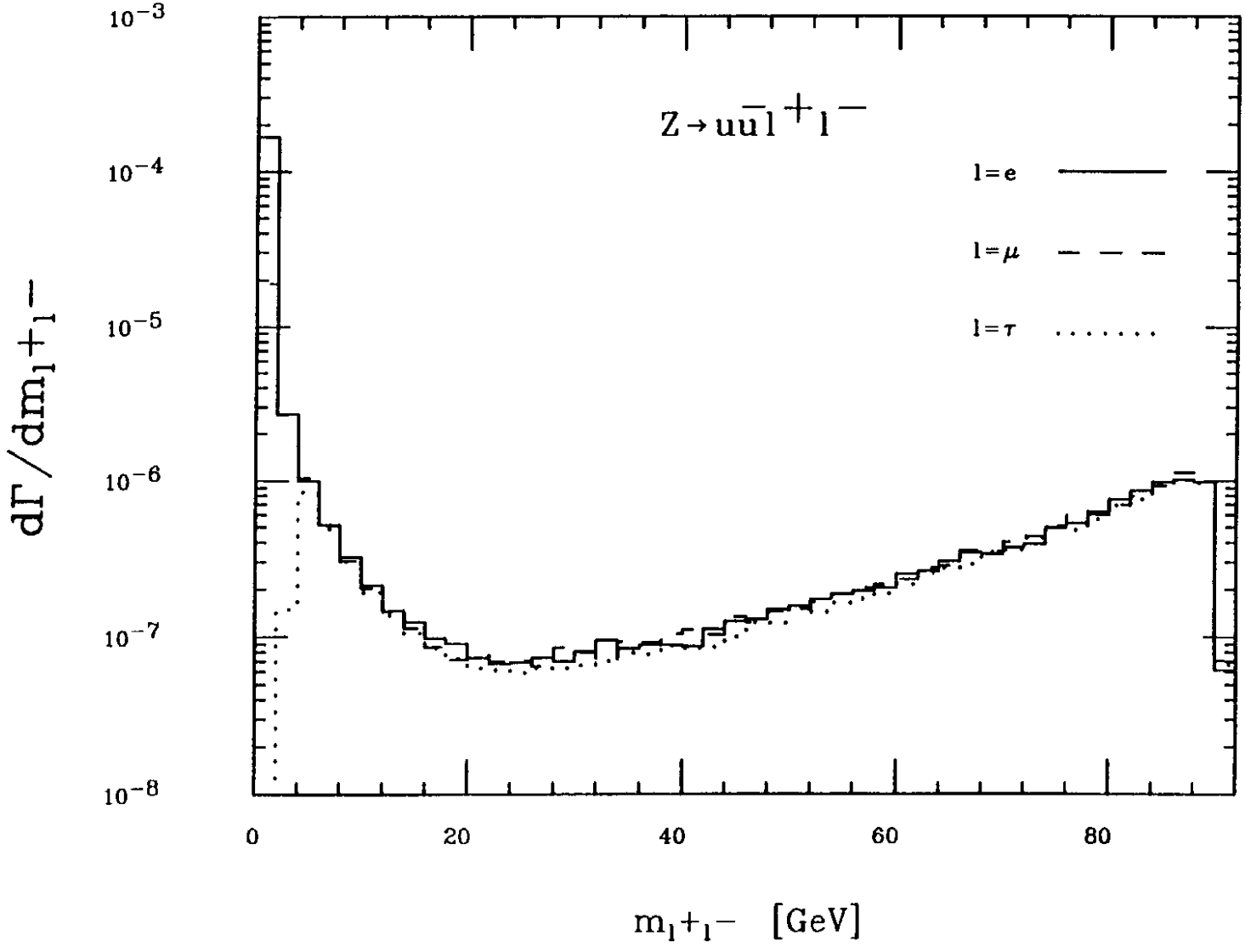
10^{-3}
10^{-4}
10^{-5}
10^{-6}
10^{-7}
10^{-8}
$d\Gamma/dm_{l^+l^-}$
$Z \to u\bar{u}l^+l^-$
l=e
l=μ
l=τ
0
20
40
60
80
$m_{l^+l^-}$ [GeV]

Fig. 2(b)

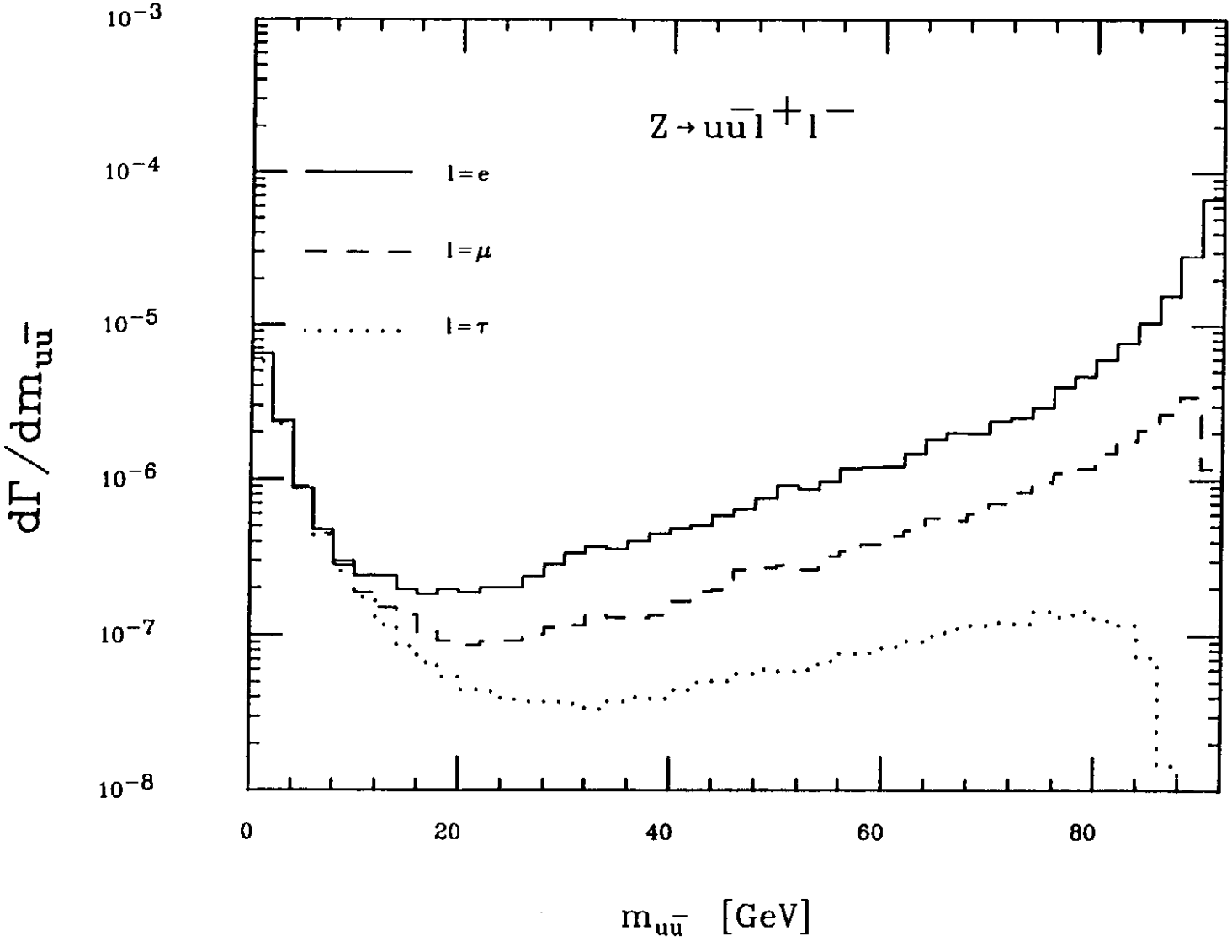
$Z \to u\bar{u}l^+l^-$
l=e
l=μ
l=τ
10^{-3}
10^{-4}
10^{-5}
10^{-6}
10^{-7}
10^{-8}
$d\Gamma/dm_{u\bar{u}}$
0
20
40
60
80
$m_{u\bar{u}}$ [GeV]

Fig. 3

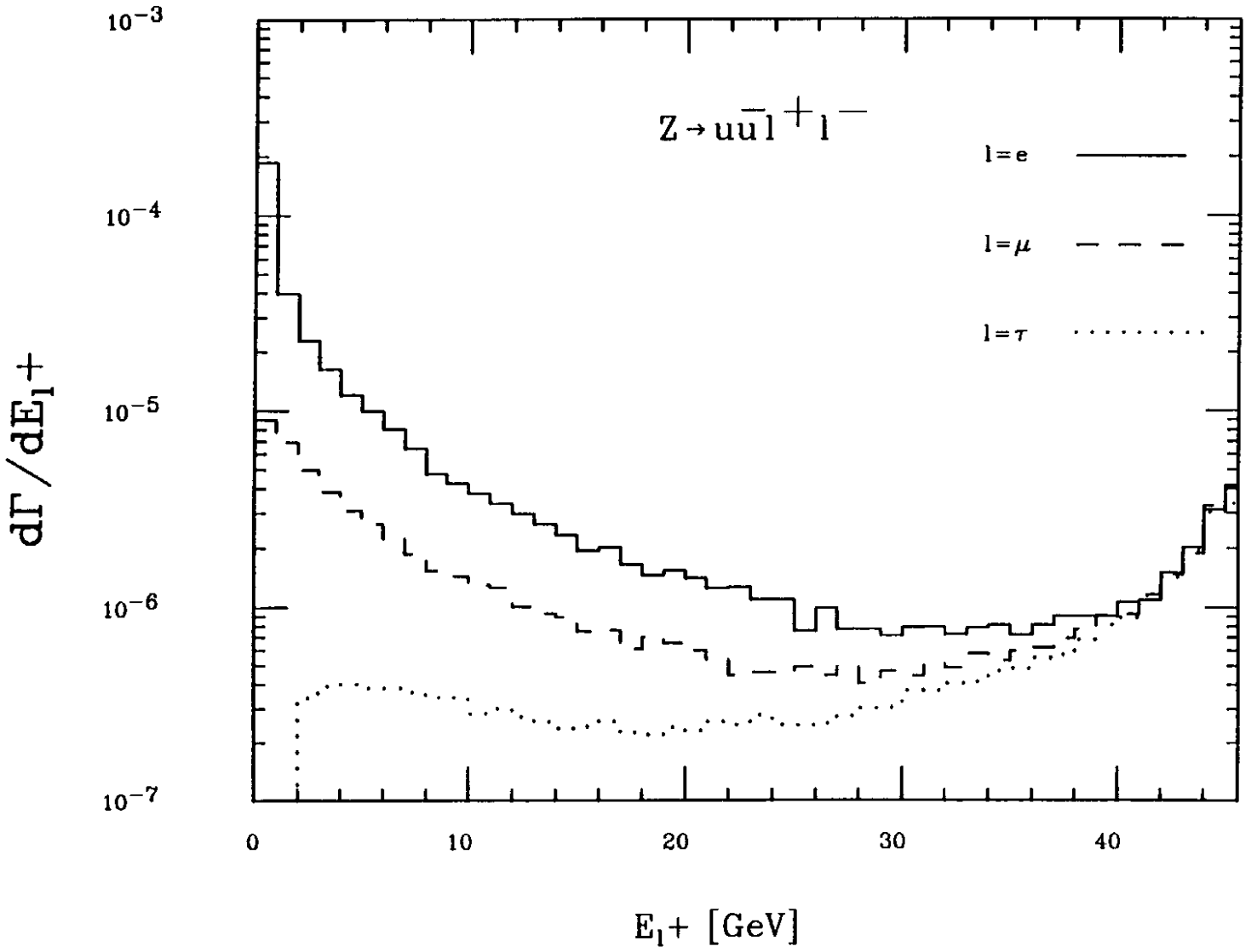
10^{-3}
10^{-4}
10^{-5}
10^{-6}
10^{-7}
$d\Gamma/dE_{l^+}$
$Z \to u\bar{u}l^+l^-$
l=e
l=μ
l=τ
0
10
20
30
40
E_{l^+} [GeV]

Fig. 4(a)

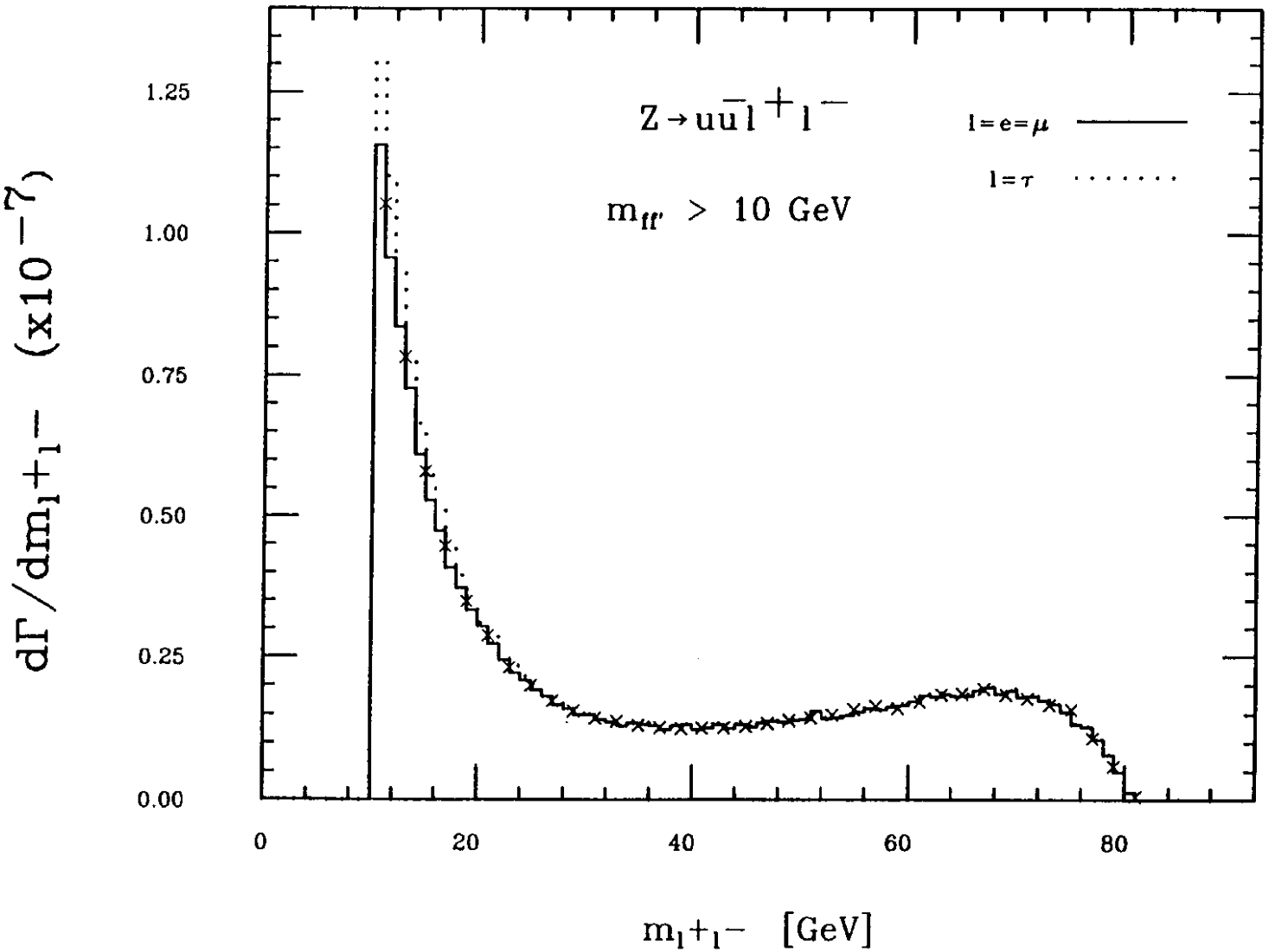
$Z \to u\bar{u}l^+l^-$
$l = e = \mu$
$l = \tau$
$m_{ll'} > 10$ GeV
$d\Gamma/dm_{l^+l^-}$ $(x10^{-7})$
1.25
1.00
0.75
0.50
0.25
0.00
0
20
40
60
80
$m_{l^+l^-}$ [GeV]

Fig. 4(b)

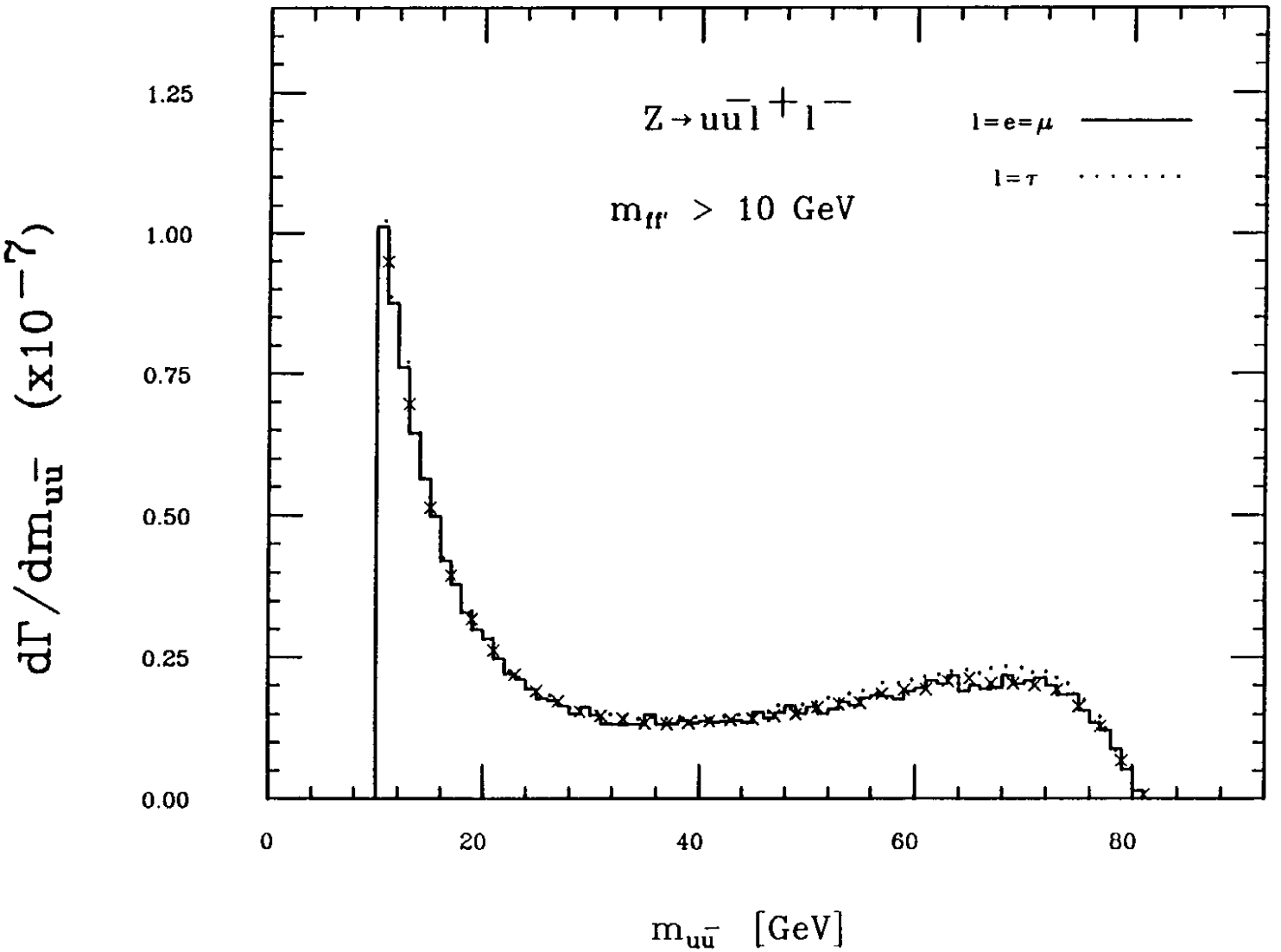
$Z \to u\bar{u}l^+l^-$
$l = e = \mu$
$l = \tau$
$m_{ll'} > 10$ GeV
$d\Gamma/dm_{u\bar{u}}$ $(x10^{-7})$
1.25
1.00
0.75
0.50
0.25
0.00
0
20
40
60
80
$m_{u\bar{u}}$ [GeV]

Fig. 5

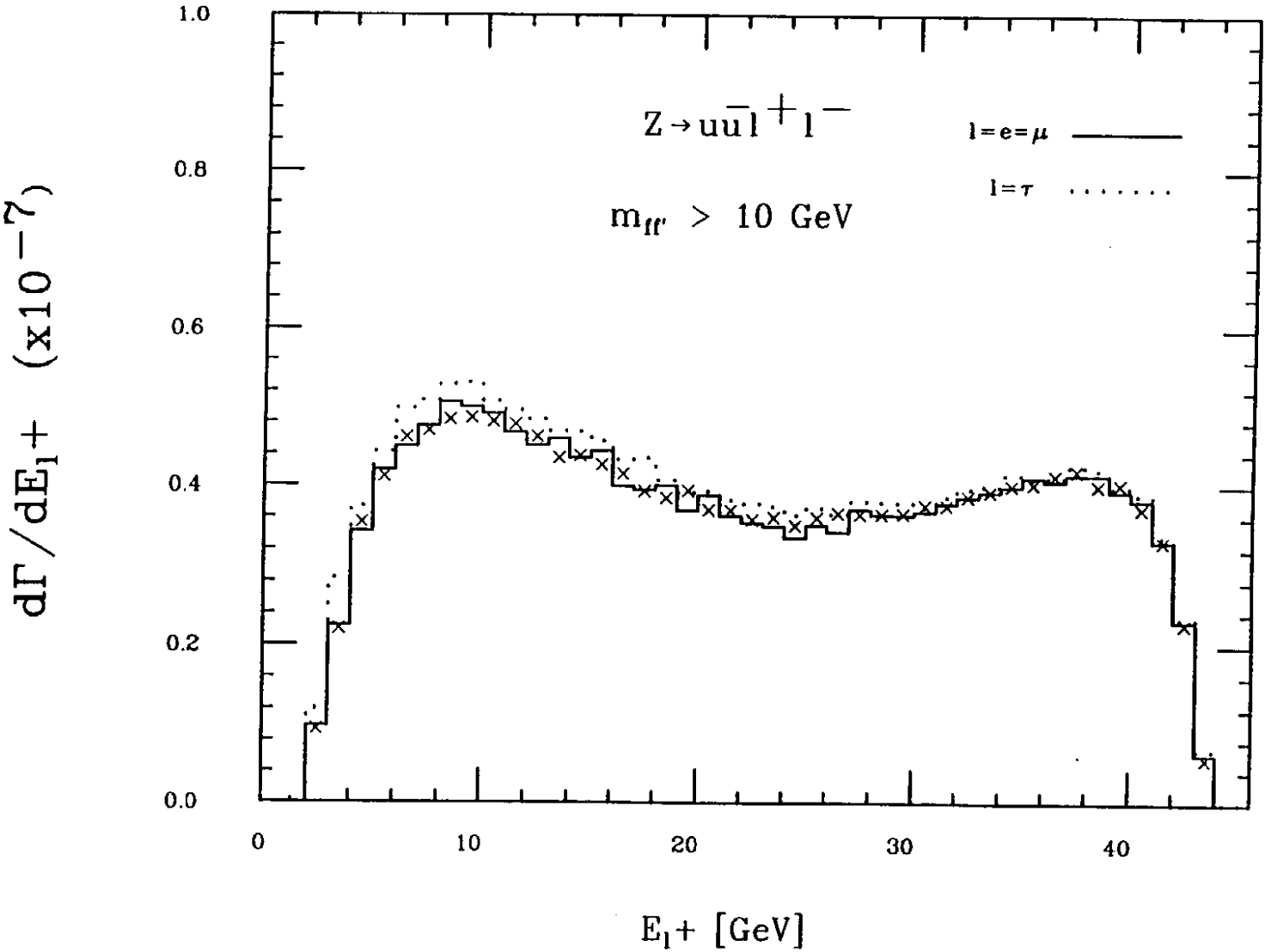
1.0
0.8
0.6
0.4
0.2
0.0
0
10
20
30
40
$Z \to u\bar{u}l^+l^-$
$l = e = \mu$
$l = \tau$
$m_{ll'} > 10$ GeV
$d\Gamma/dE_{l^+}$ (x10^{-7})
E_{l^+} [GeV]

Fig. 6

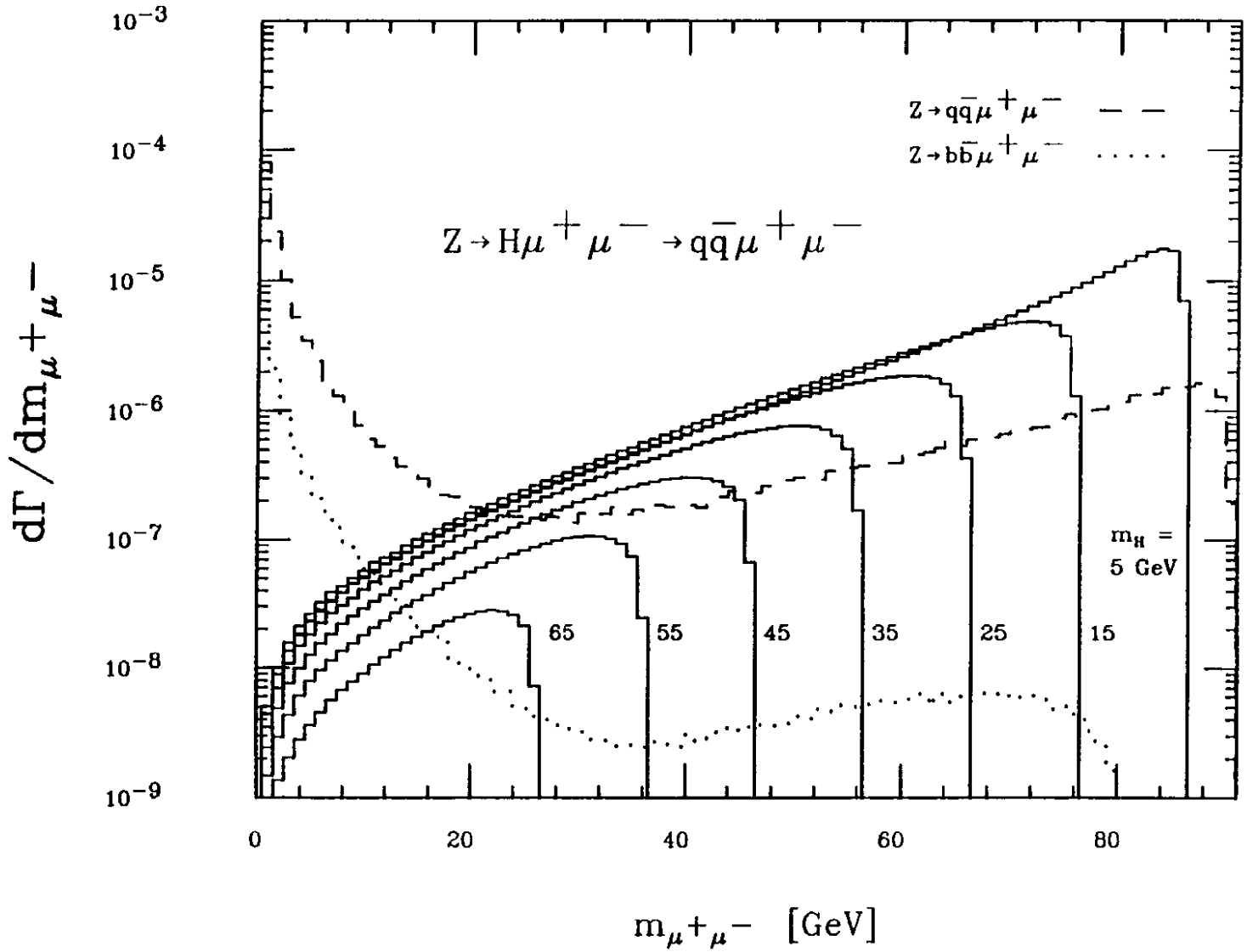
10^{-3}
10^{-4}
10^{-5}
10^{-6}
10^{-7}
10^{-8}
10^{-9}
$d\Gamma/dm_{\mu^+\mu^-}$
$Z \to q\bar{q}\mu^+\mu^-$
$Z \to b\bar{b}\mu^+\mu^-$
$Z \to H\mu^+\mu^- \to q\bar{q}\mu^+\mu^-$
m_H = 5 GeV
65
55
45
35
25
15
0
20
40
60
80
$m_{\mu^+\mu^-}$ [GeV]

Fig. 7

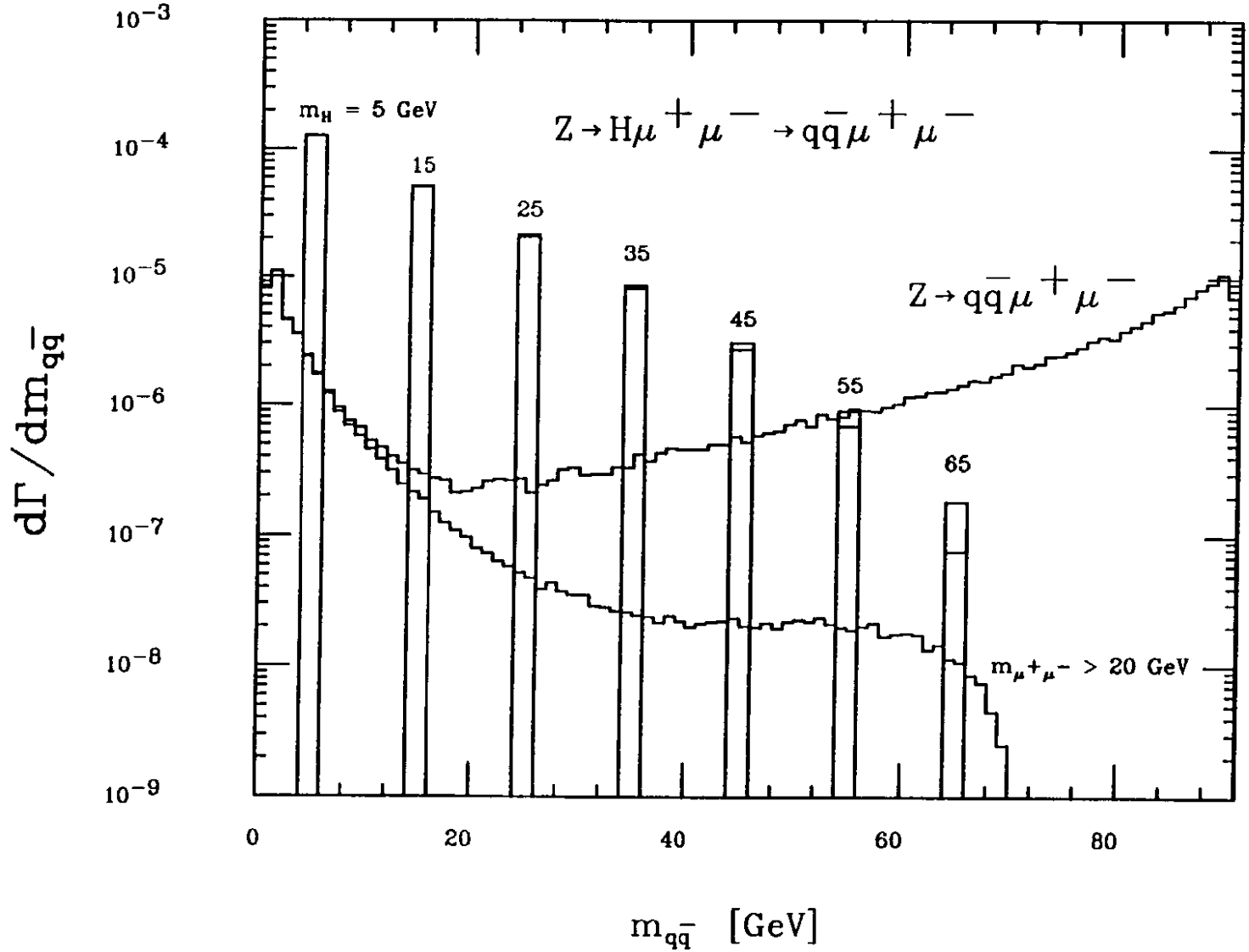
10^{-3}
10^{-4}
10^{-5}
10^{-6}
10^{-7}
10^{-8}
10^{-9}
$d\Gamma/dm_{q\bar{q}}$
m_H = 5 GeV
15
25
35
45
55
65
$Z \to H\mu^+\mu^- \to q\bar{q}\mu^+\mu^-$
$Z \to q\bar{q}\mu^+\mu^-$
$m_{\mu^+\mu^-} > 20$ GeV
0
20
40
60
80
$m_{q\bar{q}}$ [GeV]

Fig. 8

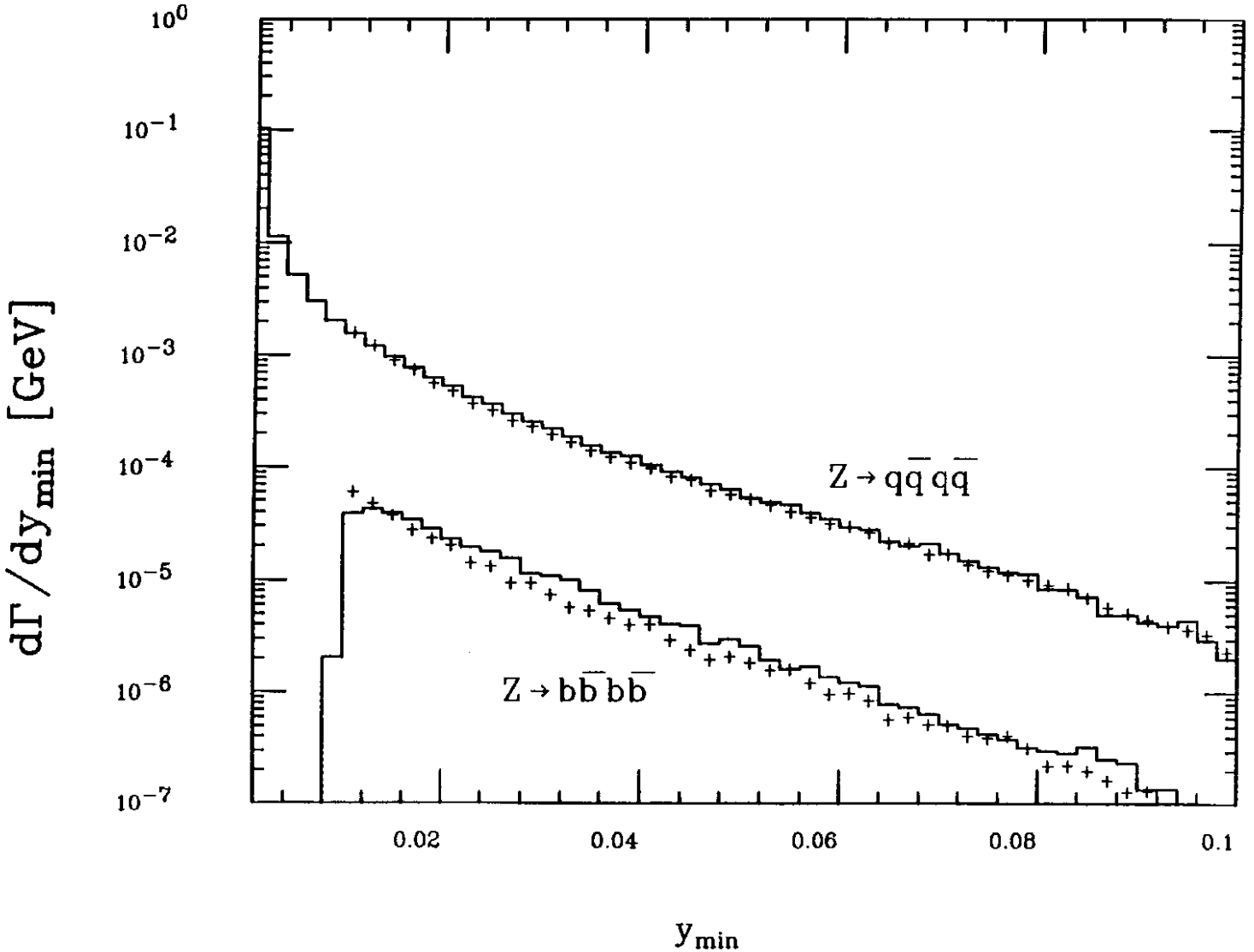
10^0
10^{-1}
10^{-2}
10^{-3}
10^{-4}
10^{-5}
10^{-6}
10^{-7}
$d\Gamma / dy_{min}$ [GeV]
$Z \to q\bar{q}\,q\bar{q}$
$Z \to b\bar{b}\,b\bar{b}$
0.02
0.04
0.06
0.08
0.1
y_{min}